# TITLE

Automatic Left Atrial Wall Segmentation from Space MRI via Advanced Two-Layer Level Sets with Distance Constraints

(Master of Science Thesis)

by

**Yuanbo JI**

July, 2017

Master Electrical Engineering Program,
Faculty of Electrical Engineering, Mathematics and Computer Science,
Delft University of Technology,
Delft, the Netherlands.

This dissertation has been approved by:

| | |
|---|---|
| Supervisor in TU Delft: | Prof. dr. ir. Boudewijn P. F. Lelieveldt |
| Supervisor in LUMC: | Dr. Ir. Rob J. van der Geest |
| Daily supervisor in LUMC: | Dr. Qian Tao |

Thesis Committee Members:

| | |
|---|---|
| Prof. dr. ir. B. P. F. Lelieveldt, | Delft University of Technology |
| Dr. J. van Gemert, | Delft University of Technology |
| Dr. Ir. Rob J. van der Geest, | Leiden University Medical Center |
| Dr. Qian Tao, | Leiden University Medical Center |



Contact Email: *yorick.cn@gmail.com*

An electronic version of this dissertation is available at
http://repository.tudelft.nl/.

*Science is a wonderful thing*
*if one does not have to earn one's living at it.*

Albert Einstein

# CONTENTS

# SUMMARY

Medical images segmentation is a key component in Diagnostic Radiology, and has a lot of clinical application areas, including disease diagnosis and surgery intervention. Accurate segmentation of medical images is still a challenge due to complicated anatomical structures and non-ideal image quality. In this thesis, aiming to solve two contours segmentation problems, a two-layer levelset method with an efficient distance constraint is proposed, which can be used to detect two contours simultaneously. With the distance constraint, not only the level set evolution at two levels is regularized, but also physical information of wall thickness can be imposed. In the proposed method, a soft distance constraint is designed to ensure that unclear boundaries in locations with poor image quality can be detected. The feasibility and reliability of the proposed distance constraint are verified. Due to the proposed distance constraint, evolution speed of the level set function around boundaries can be limited effectively, so that it is much easier for unclear boundaries to be detected. Compared to former works, the breakthrough and advantages of the proposed method are discussed and analyzed. Then, the proposed method is applied to segment advanced MRI SPACE left atrium (LA) data. Former works are also compared in implementation process. The accuracy of the proposed method is evaluated by quantitative evaluation methods, which reports that the average perpendicular distance (APD) and dice similarity coefficient (DSC) for endocardium and epicardium of LA both show a high agreement with groundtruth. Compared to manual annotation from experience observers, the proposed method achieved an APD of less than $1mm$ and a DSC of around 0.95, for the LA segmentation at both inner and outer contours. Even in locations with poor image quality, the proposed method still performs very well, which proves that the proposed method is accurate and robust. the proposed method can also be easily extended to the 3D situation. Moreover, to test flexibility and applicability of the proposed method, MRI CINE left ventricle (LV) data is used. The results show that the proposed method has an excellent performance on LV images segmentation, with an APD of less than $1.5mm$ and an DSC of 0.96, at both inner and outer contours. Therefore, the proposed method can work very well in simultaneously segmenting two contours, and has a wide range of applications in segmenting anatomical structures from medical image analysis.

**Keywords**: Image segmentation, Two-layer levelset, Distance constraint

# PREFACE

This thesis is part of Master Electrical Engineering Program at EEMCS/ Delft University of Technology, the Netherlands.

This thesis is finished in Division of Image Processing (LKEB) / Leiden University Medical Center (LUMC), the Netherlands.

*Yuanbo Ji*
*Delft, July 2017*

# 1

# INTRODUCTION

*You cannot teach a man anything;*
*You can only help him discover it in himself.*

Galileo Galilei

## 1.1. BACKGROUND

### 1.1.1. IMAGE SEGMENTATION

‘Image segmentation is the process of assigning a label to every pixel in an image such that pixels with the same label share certain characteristics.’ This is the definition about image segmentation in Wikipedia. Briefly, it aims to extract interests of objects from background or to separate different objects. It plays a key role from image processing to image analysis [1], which can be shown in Fig.1.1.

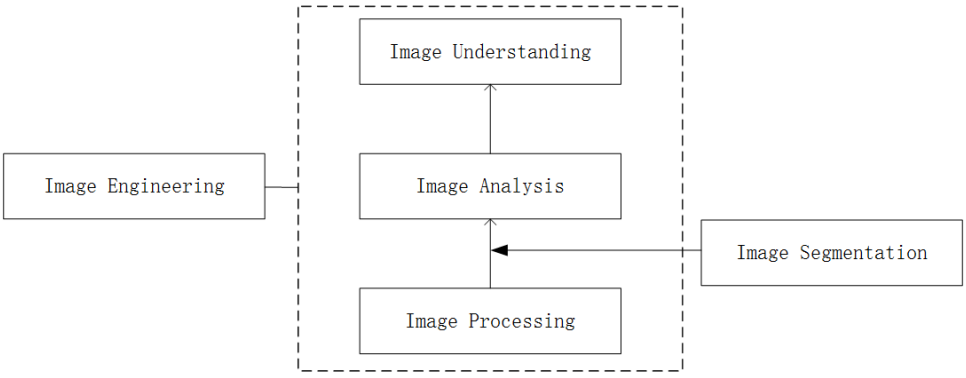


Figure 1.1: The role of image segmentation in image engineering

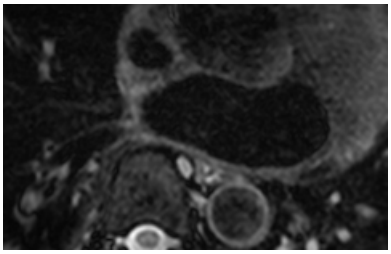

Figure 1.2: Example of LA MR SPACE image

From 70's last century, image segmentation has been a typical topic, which attracted many academic researchers. One image can be segmented with respect to some characteristics or computed properties, such as shapes, colors, intensities, or textures. Because of the complexity of images, how to accurately extract our interested information from one image becomes a hot issue. Since it is hard to represent a general characteristic for different objects from different images, there does not exist a general algorithm to suit for every image segmentation problem.

According to features of image scenes, it can be divided into the simple scene and the complex scene [2]. Images with simple scenes normally have small amount of objects and simple characteristics, such as synthetic images, non-noise images and images with uniform and homogeneous regions. In the other side, if one image has some interferences like complicated objects, unclear boundaries and nonlinear noise, the image scene can be regarded as a complex scene. And most medical images belong to complex scenes. For example, because of the inhomogeneous main magnetic field, MRI images are always inhomogeneous and have much random noise. Especially, the irregular shapes of human tissues make segmentation problems more complicated. Such interferences in complex scenes are really big challenges to image segmentation.

### 1.1.2. SPACE-MRI OF LEFT ATRIUM

Magnetic resonance imaging (MRI) is an advanced diagnostic imaging technology, which is very powerful and can show anatomic information of soft tissues. Especially, compared to traditional computed tomography (CT), MRI produces zero dose and does not have any side-effects on human body. There are many sequences available in applications of MR imaging, and different sequences can be applied to detect different diagnostic information. The novel 3D SPACE (Sampling Perfection with Application optimized Contrasts using different flip angle Evolution) MRI sequence [3] is the state-of-art technique enabling visualizing the LA wall in fine detail, as shown in Fig.1.2.

## 1.2. MOTIVATION FOR LEFT ATRIAL WALL SEGMENTATION

Atrial fibrillation (AF) originating from the left atrium (LA) is the most common cardiac electrophysiological disorder worldwide. The anatomical structure of LA is shown in Fig.1.3. Tissue characteristics of the LA wall can provide valuable information for determining the treatment strategy for AF patient [4]. Segmentation of the LA walls from

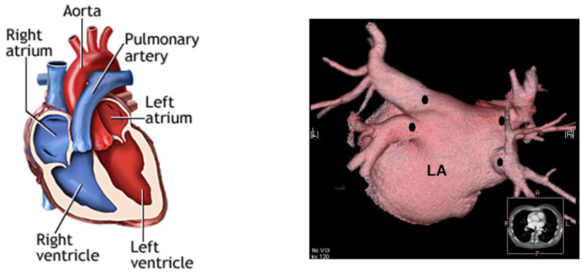


Figure 1.3: Anatomic structure of LA

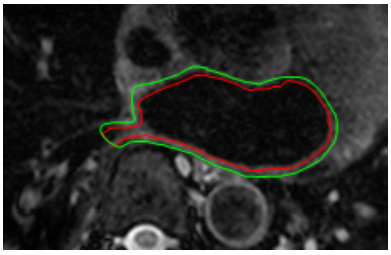

Figure 1.4: Example of Manual delineated LA SPACE MR image

SPACE MRI is of a high clinical interest.

In clinical research, the inner wall of LA is named endocardium, and the outer wall of LA is named epicardium. Traditionally, the endocardial contour and the epicardial contour are both delineated by experts, as shown in Fig.1.4. It always consumes a lot of time, and heavily relies on subjective judgment and experience of radiologists. If there is a method to detect the inner wall and outer wall of LA automatically, the efficiency of diagnostic process will definitely increase and the workload of radiologists will be released in a big degree.

## 1.3. RESEARCH CHALLENGE

Although the SPACE MRI sequence already has an excellent performance in imaging Left Atrium walls, the image is still not a perfect one to analyze and there exist some interference. As shown in Fig.1.2, apart from the noise, there are so many nearby objects, which can be considered as interference to extract endocardium and epicardium of LA. Due to the empty visualization of LA cavity, it is not difficult to detect endocardium, and some applications have been used in [5]. However, unlike short-axis Left Ventricle MR images with high quality and regular shapes, in most cases, boundaries between epicardium of LA and background are not clear, which are hard to be recognized. Moreover, the irregular shape and small thickness of LA walls increase the difficulty of segmentation. Therefore, how to extract endocardium and epicardium of LA simultaneously becomes a tough challenge.

## 1.4. OBJECTIVES

Aiming to extract two layers of LA wall simultaneously, an efficient algorithm should been designed, which would generate desirable distance constraints between two contours. The algorithm should work well in the 2D situation and could be extended to 3D volumes. Moreover, the method should have an excellent performance in validation on different datasets.

## 1.5. OUTLINES

This thesis is combined with five chapters.

Chapter 1 gives a brief overview of image segmentation problems and our special SPACE-MR LV images. The challenge and objectives of this thesis are also described.

Chapter 2 describes the reason why level set methods are chosen to solve our segmentation problems. Some classic and common level set methods are demonstrated.

Chapter 3 proposes the mathematical theory of our two-layer level set method with the distance constraint. The parameters in our method are analyzed in detail. Compared to former works, the breakthrough and advantages of our method are explained. Moreover, the validation on a synthetic image of our method is verified.

Chapter 4 presents the implementation of our method on *in vivo* data. The feasibility and robustness of the proposed distance constraint are proved, and the accuracy of our method is compared with other state-of-art methods. The quantitative evaluations of segmentation on training datasets and validation datasets are demonstrated. Furthermore, our method is extended to LV images segmentation, and the results are reported.

Chapter 5 gives a brief conclusion of the whole thesis work.

# REFERENCES

[1] M. Sonka, V. Hlavac, and R. Boyle, *Image processing, analysis, and machine vision* (Cengage Learning, 2014).

[2] H. Delingette, M. Hebert, and K. Ikeuchi, *Shape representation and image segmentation using deformable surfaces,* Image and vision computing **10**, 132 (1992).

[3] B. Baumert, K. Wörtler, D. Steffinger, G. Schmidt, M. Reiser, and A. Baur-Melnyk, *Assessment of the internal craniocervical ligaments with a new magnetic resonance imaging sequence: three-dimensional turbo spin echo with variable flip-angle distribution (space)*. Magn Reson Imaging **27**, 954 (2009).

[4] N. F. Marrouche, D. Wilber, G. Hindricks, P. Jais, N. Akoum, F. Marchlinski, E. Kholmovski, N. Burgon, N. Hu, L. Mont, *et al.*, *Association of atrial tissue fibrosis identified by delayed enhancement mri and atrial fibrillation catheter ablation: the decaaf study,* Jama **311**, 498 (2014).

[5] Q. Tao, E. G. Ipek, R. Shahzad, F. F. Berendsen, S. Nazarian, and R. J. van der Geest, *Fully automatic segmentation of left atrium and pulmonary veins in late gadolinium-enhanced mri: Towards objective atrial scar assessment,* Journal of Magnetic Resonance Imaging **44**, 346 (2016).

# 2

# DESCRIPTION OF LEVEL SETS

## 2.1. WHY USING LEVEL SET METHODS

THERE are several classical image segmentation methods, including thresholding, region break and merge, and edge detection [1]. Compared to these traditional methods, level set methods have some outstanding advantages. First, because level set methods are based on a energy minimization framework, it is easy to be formulated and generate prior information into the energy function [2]. Then, level set methods can handle topology changes very well [3] and promise smoothness of evolution curves, which means that level set can be applied to segment objects with complicated structures, such as human organs. Combined with features of our SPACE MR images, it is possible for level set methods to adapt to segment LA walls with irregular shapes. Especially, some constraints, such as average LA wall physical thickness, are able to be generated into the solution solving process.

The level set method can deal with complex 2D/3D structures without explicitly specifying the object shape. Therefore, level set methods would be the first choice to deal with our problem. Next, in the following part of this chapter, the advantages of level set methods will be introduced in detail.

## 2.2. DEVELOPMENT OF LEVEL SET METHODS

Level set methods were first proposed by Osher and Sethian in 1988 to solve hydromechanics problems [4]. Level set methods was introduced to image segmentation area from 90's last century [5], which played an important role in geometric active contour model. Compared to Snake model which is called parametric active contour model [6], contours in level set methods are not represented as parameterized curves and not limited by topological changes [7]. It means that level set methods can detect several objects simultaneously without prior information, and can decrease calculation complexity.

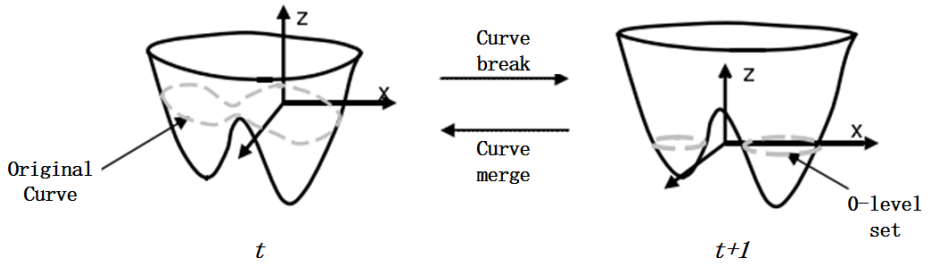


Figure 2.1: Implicit expression and topology changes of curve

### 2.2.1. BASIS OF LEVEL SET METHODS

In level set methods, geometric active contours are represented implicitly as level sets function.

#### MATHEMATIC EXPRESSION OF GEOMETRIC ACTIVE CONTOUR MODEL

A parameterized 2D curve can be explicitly represented as $C(s,t) = \big(x(s,t), y(s,t)\big)$, where $s$ is arc length parameter, and $t$ is time. $\vec{N}$ represents unit normal vector of curve $C$, so that the following partial differential equation (PDE) can be used to represent evolution process of $C$ towards $\vec{N}$ direction:

$$\frac{\partial C}{\partial t} = F(C)\vec{N} \tag{2.1}$$

where $F(C)$ is the evolution speed of curve $C$ towards $\vec{N}$. This curve evolution model has two main problems: (1) Because of the discontinuity of curve, it is not easy to get an accurate solution from PDE; (2) Since topological changes of parametric curves are limited, the range of model applications is heavily constrained [4].

To solve above problems, level set function is introduced.

In order to represent $C$ implicitly, a level set function can be defined as $\phi(x,y,t) : R^2 \times R^+ \rightarrow R$, which is a signed distance function. It can be said that curve $C$ varies with function $\phi$ . Therefore, there is

$$\begin{cases} C(0) = \{(x,y) \mid \phi(x,y,0) = 0\} \\ C(t) = \{(x,y) \mid \phi(x,y,t) = 0\} \end{cases} \tag{2.2}$$

In Eq. 2.2, closed curve $C$ is represented by 0-level set of function $\phi$, so that the curve evolution problem is converted to analysis of level set function $\phi$. Implicit expression and topology changes of curve is shown at Fig.2.1.

Therefore, the evolution PDE equation of level set function $\phi$ can be written as:

$$\frac{\partial \phi}{\partial t} = F\left|\nabla\phi\right| \tag{2.3}$$

which is Hamilton–Jacobi equation [8] and also called level set equation [4]. Eq.2.3 promises that active contour $C$ is always 0-level set of function $\phi$, $\{\phi(C,t) = 0\}$.

#### DEFINITION OF LEVEL SET FUNCTION

In traditional level set methods, implicit function $\phi$ is defined as a signed distance function, which satisfies $\left|\nabla\phi\right| = 1$ [3]. Set $\overrightarrow{X} = (x, y)$ as one arbitrary pixel in 2D image domain $\Omega$, $\overrightarrow{X_C}$ represent pixel sets in closed curve $C$, so that the minimum Eulerian distance between $\overrightarrow{X}$ and curve $C$ is :

$$d\left(\overrightarrow{X}\right) = min\left(\overrightarrow{X} - \overrightarrow{X_C}\right), \overrightarrow{X} \in \Omega \tag{2.4}$$

If $R_1$ represents inside region of curve $C$ and $R_2$ represents outside region of curve $C$, curve $C$ can be implicitly represented by a Lipschitz continuous level set function $\phi\left(\overrightarrow{X}\right)$, and $\left|\phi\left(\overrightarrow{X}\right)\right| = d\left(\overrightarrow{X}\right)$. There is:

$$\phi\left(\overrightarrow{X}\right) = \begin{cases} +d\left(\overrightarrow{X}\right) & \text{if } \overrightarrow{X} \in R_1 \\ 0 & \text{if } \overrightarrow{X} \in \overrightarrow{X_C} \\ -d\left(\overrightarrow{X}\right) & \text{if } \overrightarrow{X} \in R_2 \end{cases} \tag{2.5}$$

Since implicit function $\phi(x, y)$ varies with time $t$, one dimension higher level set function $\phi(x, y, t)$ is produced. However, during the process of curve evolution, level set function $\phi$ could derive sharp shape or shocks, which has a very negative effect on further computation. In other words, because of the discrete of digital images and noises, level set function may lose signed distance characteristic. To solve this problem, function $\phi$ should be reinitialized periodically to keep it as a signed distance function [5]. Several methods have been proposed to solve the re-initialization problem [5, 7, 9], but it has a heavy influence on speed of curve evolution and accuracy of solution [10]. It means that if possible, re-initialization should be avoided. Li [11] first proposed an advanced level set method without re-initialization in 2005, which is based on a new variational formulation. The method was perfected and named as DRLSE (Distance Regularized Level Set Evolution) in 2010 [12]. Li's method creatively generated an energy term $\left(\left|\nabla\phi\right| - 1\right)^2$ into the level set energy minimization framework to force $\left|\nabla\phi\right|$ close to 1, which avoids re-initialization perfectly.

### 2.2.2. COMMON APPLICATIONS OF LEVEL SET METHODS

Current level sets methods can be divided into two categories. One is edge-based method, which depends on information along edges between objects. The other one is region-based method, which focuses on region information of different objects.

#### EDGE-BASED

Edge information was first applied in level set methods, and it is mainly based on gradient information of image [13, 14]. Here a popular edge-based level set model is introduced. If $I(x, y)$ is an image, a new edge indicator function can be defined as:

$$g = \frac{1}{1 + |\nabla G * I|^2} \tag{2.6}$$

where $G$ is Gaussian kernel. Gradient information of image $I$ is embedded in function $g$. When $I$ has a big gradient, corresponding function $g$ will have a small value. An energy functional can be defined as:



$$\varepsilon = L + A \tag{2.7}$$

where $L$ is the length term, and $A$ is acceleration term. With level set function $\phi(x, y)$, these two terms is defined as:

$$L = \lambda \int_I g\delta(\phi) \left|\nabla\phi\right| dxdy \tag{2.8}$$

$$A = \upsilon \int_I gH(-\phi)\, dxdy \tag{2.9}$$

where $\lambda > 0$ and $\upsilon$ are weighting coefficients, $\delta(\phi)$ is Dirac function, $H(\phi)$ is Heaviside function. When minimizing the energy functional, length term calculates 0 level contour length and smoothes the curve, and $g$ in this term is to guide 0 level contour move towards object boundaries. In acceleration term, because $\int H(-\phi)\, dxdy$ computes the area of inside region of 0 level contour, $\upsilon > 0$ can control 0 level contour to shrink and $\upsilon < 0$ can control 0 level contour to expand. When 0 level contour is close to object boundaries with big gradients, function $g$ with small values will slow down the expanding or shrinking evolution process, which stop 0 level curve to be over-evoluted.

This edge-based method can be extended to a level set method without re-initialization [11]. Only an extra regularization term is required in the extended method, which is:

$$R = \mu \int_I \frac{1}{2} \left(\left|\nabla\phi\right| - 1\right)^2 dxdy \tag{2.10}$$

where $\mu > 0$ is weighting coefficient.

Therefore, according to gradient descent method, solutions to minimization of the energy functional is $\frac{\partial\phi}{\partial t} = -\frac{\partial\varepsilon}{\partial\phi}$, with $\frac{\partial\varepsilon}{\partial\phi} = \frac{\partial L}{\partial\phi} + \frac{\partial A}{\partial\phi} + \frac{\partial R}{\partial\phi}$. The final evolution equation is obtained as:

$$\frac{\partial\phi}{\partial t} = \lambda\delta(\phi)\, div\left(g\frac{\nabla\phi}{\left|\nabla\phi\right|}\right) + \upsilon g\delta(\phi) + \mu\left(\nabla^2\phi - div\left(\frac{\nabla\phi}{\left|\nabla\phi\right|}\right)\right) \tag{2.11}$$

And the evolution time step $\triangle t$ should satisfy Courant-Friedrichs-Lewy (CFL) condition $\mu\triangle t \le h^2/4$ [12, 15], where the space step $h = 1$ in computer system. Therefore, there is $\mu\triangle t \le 1/4$.

In traditional reinitialization level set methods, in order to realize the regularization of level set function, $\left|\nabla\phi\right|$ is enforced to be 1 in every iteration time. In Li's method in [11], $\left|\nabla\phi\right|$ is encouraged to be close to 1, but not enforced. However, Li's method shows an excellent performance, which means that his method can be used to replace the traditional reinitialization process of level set functions.

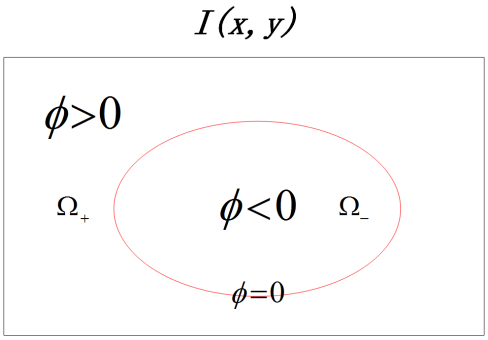


Figure 2.2: Domain representation of Level set method



### REGION-BASED

The first region-based level set method was proposed by Chan and Vese in 2001, which is called piecewise constant model (PC) [3]. After that, many other region-based methods were developed, such as piecewise smooth model (PS) [16] and Markov random field driven region-based model [17]. Among these such many methods, PC and PS, as two classical region-based models, will be introduced in this thesis.

**PC Model** Piecewise constant model is named from piecewise constant function. For an image $I$ on domain $\Omega$, $(x, y)$ is an arbitrary pixel on $I$. Let $\Omega_-$ represents inside region of contour $C$, $\Omega_+$ represents outside region of contour $C$, so that there is energy functional:

$\varepsilon = \lambda_1 \int_{\Omega_-} |I(x,y) - c_1|^2 dxdy + \lambda_2 \int_{\Omega_+} |I(x,y) - c_2|^2 dxdy + v|C|$

where $\lambda_1$, $\lambda_2$, $v$ are weighting coefficients, $c_1$, $c_2$ are two constants that estimate average image intensity in domain $\Omega_-$ and $\Omega_+$, respectively. The last term is to smooth the contour $C$. The function of first two data fitting terms is more like the function of standard deviation in mathematics, which computes errors. If the 'standard deviation' gets the minimum value, the object can be extracted accurately from background.

Compared to Edge-based methods, PC model has a good performance on segmenting objects without clear boundaries. However, since PC model is based on global information of image $I$, it has a very high requirement to homogeneity of domain $\Omega_-$ and $\Omega_+$. It means that PC model can only show a good performance on images with simple scenes, and is not applicable to inhomogeneous images.

This PC model can be easily introduced into level set method by adding level set function, as show in Fig.2.2. And the level set function is embedded in the Heaviside function $H(\phi)$, where $1 - H(\phi)$ represents domain $\Omega_-$ and $H(\phi)$ represents $\Omega_+$.

**PS Model** In order to overcome the disadvantages of PC model, PS model was proposed, which can be used to segment inhomogeneous images [16]. Similar to parameters in PC model, an image $I(x, y)$ and two subdomains $\Omega_-$ and $\Omega_+$ are also defined in PS model. However, two new smooth functions need to be introduced here, which

are $u^-(x,y)$ in domain $\Omega_-$ and $u^+(x,y)$ in domain $\Omega_+$ . The energy functional can be expressed as:

$$\varepsilon = \lambda_1 \int_{\Omega_+} \left|u^+ - I\right|^2 dxdy + \lambda_2 \int_{\Omega_-} |u^- - I|^2 dxdy + \mu \int_{\Omega_+} \left|\nabla u^+\right|^2 + \mu \int_{\Omega_-} |\nabla u^-|^2 + v|C|$$

where $\lambda_1$, $\lambda_2$, $\mu$, $v$ are weighting coefficients. The first two terms are data fitting term, the third and forth terms are smoothing terms to smooth $u^+$ and $u^-$, the last term is the smoothing term to keep contour $C$ be smooth. The smooth functions $u^+$ and $u^-$ can be obtained by minimizing the energy functional respect to $u^+$ and $u^-$, respectively. Since functions $u^+$ and $u^-$ also have a denoising effect in their corresponding domain, PS has the ability to resist inhomogeneity and processes images with complex scenes.

Similar to PC model, PS model also can be easily extended to level set methods by generating Heaviside function with level set function.

PS model also has obvious drawbacks [18]. Besides updating $\phi$ by solving PDE, smoothing functions $u^+$ and $u^-$ are also required to be updated by solving two PDEs in each iteration time. This heavily increases the computational complexity, which means that computation process will consume a lot of time. Therefore, it is not easy to apply PS model in practice.

### MULTIPHASE LEVEL SETS

Normally, if only one object need to be extracted, one 0-level set of one level set function is required. However, in many cases, there are more than 2 objects to be extracted, and 0-level set of one level set function is not enough to represent all objects. To solve this problem, there are two methods. One uses multiple level sets of single level set function to represent different contours. The other one uses 0-level set of multiple level set functions to detect different objects.

Chan and Vese proposed a creative framework to solve segmentation problems when more than two regions need to be segmented [16]. How to represent different regions with limited level set functions is the key of this framework. Now, assume that the image $I(x,y)$ has two objects with junctions, and two level set functions $\phi_1$, $\phi_2$ will be used. Therefore, each region can be expressed in Fig.2.3, where the red curve represents 0 level set of $\phi_1$, and the green curve represents 0 level set of $\phi_2$. Based on signed features of $\phi_1$, $\phi_2$, images can be represented as four subdomains: $\{\Omega_{00} : \phi_1 > 0, \phi_2 > 0\}$, $\{\Omega_{01} : \phi_1 > 0, \phi_2 < 0\}$, $\{\Omega_{10} : \phi_1 < 0, \phi_2 > 0\}$, $\{\Omega_{11} : \phi_1 < 0, \phi_2 < 0\}$.

Based on PC model, there is the level set energy functional:

$$\begin{aligned}\varepsilon = \lambda_1 \int_\Omega (I - c_{11})^2 \left(1 - H\left(\phi_1\right)\right)\left(1 - H\left(\phi_2\right)\right) dxdy + \lambda_2 \int_\Omega (I - c_{10})^2 \left(1 - H\left(\phi_1\right)\right)\left(H\left(\phi_2\right)\right) dxdy \\ + \lambda_3 \int_\Omega (I - c_{01})^2 \left(H\left(\phi_1\right)\right)\left(1 - H\left(\phi_2\right)\right) dxdy + \lambda_4 \int_\Omega (I - c_{00})^2 \left(H\left(\phi_1\right)\right)\left(H\left(\phi_2\right)\right) dxdy \\ + v_1 \int_\Omega \left|\nabla H\left(\phi_1\right)\right| + v_2 \int_\Omega \left|\nabla H\left(\phi_2\right)\right|\end{aligned} \tag{2.12}$$

where $\lambda_1$, $\lambda_2$, $\lambda_3$, $\lambda_4$, $v_1$, $v_2$ are weighting coefficients, $c_{11}$, $c_{10}$, $c_{01}$, $c_{00}$ are estimated constants of average image intensities in corresponding subdomains.

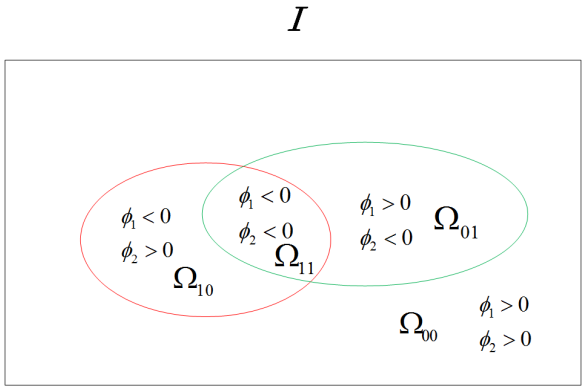


Figure 2.3: Multiplephase representation of several level set functions

By minimizing Eq.2.3, two 0 level sets of two corresponding level set functions can be obtained. Different weighting coefficients in each level set function can be modified to detect different types of objects.

If there are $N$ level set functions, $2^N$ objects can be represented at most. Based on this multiphase level sets framework, other methods like PS model can also be easily used.

However, sometimes there are some constraints or connections among different objects. These constraints or connections can be considered as the prior information. If they can be taken advantages in our methods, the accuracy must be increased. But how to embed constraints or connections among different level set functions remains a challenge.

Besides this framework, the other one with only one level set function is also an ideal framework. The basic idea of this is to use several level sets (0,1,2...) of one level set function to represent different objects. This framework will be used in our method, which is going to be described concretely later.

# REFERENCES


[1] N. R. Pal and S. K. Pal, *A review on image segmentation techniques,* Pattern recognition **26**, 1277 (1993).

[2] Y. Chen, H. D. Tagare, S. Thiruvenkadam, F. Huang, D. Wilson, K. S. Gopinath, R. W. Briggs, and E. A. Geiser, *Using prior shapes in geometric active contours in a variational framework,* International Journal of Computer Vision **50**, 315 (2002).

[3] T. F. Chan and L. A. Vese, *Active contours without edges,* IEEE Transactions on image processing **10**, 266 (2001).

[4] S. Osher and J. A. Sethian, *Fronts propagating with curvature-dependent speed: algorithms based on hamilton-jacobi formulations,* Journal of computational physics **79**, 12 (1988).

[5] R. Malladi, J. A. Sethian, and B. C. Vemuri, *Shape modeling with front propagation: A level set approach,* IEEE transactions on pattern analysis and machine intelligence **17**, 158 (1995).

[6] M. Kass, A. Witkin, and D. Terzopoulos, *Snakes: Active contour models,* International journal of computer vision **1**, 321 (1988).

[7] J. A. Sethian *et al., Level set methods and fast marching methods,* Journal of Computing and Information Technology **11**, 1 (2003).

[8] G. Aubert and P. Kornprobst, *Mathematical problems in image processing: partial differential equations and the calculus of variations*, Vol. 147 (Springer Science & Business Media, 2006).

[9] M. Sussman and E. Fatemi, *An efficient, interface-preserving level set redistancing algorithm and its application to interfacial incompressible fluid flow,* SIAM Journal on scientific computing **20**, 1165 (1999).

[10] D. Peng, B. Merriman, S. Osher, H. Zhao, and M. Kang, *A pde-based fast local level set method,* Journal of computational physics **155**, 410 (1999).

[11] C. Li, C. Xu, C. Gui, and M. D. Fox, *Level set evolution without re-initialization: a new variational formulation,* in *Computer Vision and Pattern Recognition, 2005. CVPR 2005. IEEE Computer Society Conference on*, Vol. 1 (IEEE, 2005) pp. 430–436.

[12] C. Li, C. Xu, C. Gui, and M. D. Fox, *Distance regularized level set evolution and its application to image segmentation,* IEEE transactions on image processing **19**, 3243 (2010).

[13] V. Caselles, F. Catté, T. Coll, and F. Dibos, *A geometric model for active contours in image processing,* Numerische mathematik **66**, 1 (1993).

[14] V. Caselles, R. Kimmel, and G. Sapiro, *Geodesic active contours,* International journal of computer vision **22**, 61 (1997).

[15] G. Gilboa, N. Sochen, and Y. Y. Zeevi, *Forward-and-backward diffusion processes for adaptive image enhancement and denoising,* IEEE transactions on image processing **11**, 689 (2002).

[16] L. A. Vese and T. F. Chan, *A multiphase level set framework for image segmentation using the mumford and shah model,* International journal of computer vision **50**, 271 (2002).

[17] J. Xu, J. P. Monaco, and A. Madabhushi, *Markov random field driven region-based active contour model (maracel): application to medical image segmentation,* in *International Conference on Medical Image Computing and Computer-Assisted Intervention* (Springer, 2010) pp. 197–204.

[18] C. Li, C.-Y. Kao, J. C. Gore, and Z. Ding, *Minimization of region-scalable fitting energy for image segmentation,* IEEE transactions on image processing **17**, 1940 (2008).

# 3

# THEORY OF TWO LAYER LEVEL SET METHOD

This chapter introduces our method concretely, including mathematics theory and application to synthetic images. Breakthrough work in our method compared to former methods is also described.

## 3.1. PROBLEM ANALYSIS AND CHALLENGES

As shown in Fig.1.2, the complexity of Left Atrium structure heavily increases difficulty of the segmentation problem. Besides irregular shapes of LA walls, there are also other interferences in the segmentation process, including nearby objects and unclear boundaries between outer wall and background. Image quality is also an important factor.

Because of the sufficient data library and high image quality with mature imaging technique, current double-walls segmentation normally focuses on the left ventricle (LV) walls. However, compared to SPACE-MR images of LA, short-axis LV images have a higher quality and less interference objects around LV walls, as shown in Fig.3.1. The shape of short-axis LV is also relatively regular, which is close to a circle. Moreover, the thickness of LV walls is about 4 times of LA walls, which means that LV walls have a bigger tolerance to segmentation errors than LA. Therefore, the problem of LA walls segmentation is more complicated and much tougher, and it is impossible to apply any current methods directly to deal with this LA walls segmentation problem.

However, as shown in Fig.3.1, there is a common point between LV walls and LA walls, which is that inner wall (epicardium) contours are contained in outer wall (endocardium) contours. This leaves us possibility to continue our work based on former research work. Moreover, an idea of the level set framework in [1] could be studied and transferred into our method.

In physiology, there is useful prior information of LA walls. The thickness of human LA walls is typically in a fixed range, which can be considered as a physical constraint. If

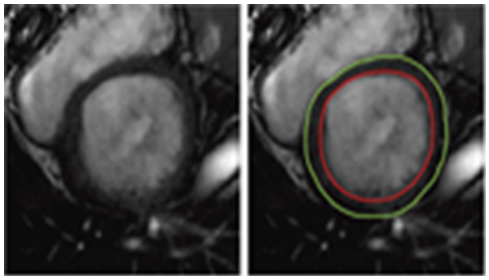

(a) A short-axis MR LV image (left row) and inner (red) and outer (green) wall contours of LV (right row) [1]

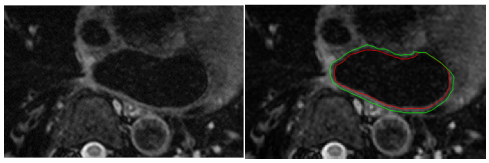

(b) A SPACE-MR LA image (left row) and inner (red) and outer (green) wall contours of LA (right row)

Figure 3.1: Examples of short-axis LV image and SPACE-MR LA image

this constraint can be introduced in our method, it will be very useful to the final results.

## 3.2. FRAMEWORK DEFINITION

Let an image $I$ defined on a domain $\Omega \subset \Re^2$, and $\mathbf{x}$ is one arbitrary pixel on $I$ with $\mathbf{x} \in I$. By defining one level set function and setting two threshold, we are able to simultaneously identify two contours, the endocardial and epicardial left atrial wall. The level set function $\phi$ is defined on domain $\Omega \subset \Re$. 0-level and k-level contours represent inner wall and outer wall of LA, which are defined as $C_0 = \{\mathbf{x} : \phi(\mathbf{x}) = 0\}$ and $C_k = \{\mathbf{x} : \phi(\mathbf{x}) = k\}$ respectively. In our method, value of $\phi$ in region inside inner wall is set to below zero. Because $C_0$ and $C_k$ are two closed contours, domain $\Omega$ is divided into 3 parts, $\Omega_1 = \{\mathbf{x} : \phi(\mathbf{x}) < 0\}$, $\Omega_2 = \{\mathbf{x} : 0 < \phi(\mathbf{x}) < k\}$, $\Omega_3 = \{\mathbf{x} : \phi(\mathbf{x}) > k\}$, as shown in Fig.3.2.

In order to distinguish different regions during evolution process, Heaviside function $H$ is introduced here. Normal heaviside function $H$ is not enough for recognizing three regions, so that a 'new-heaviside' function can be organized as $M_i(\phi(\mathbf{x})) = 1$ for $\mathbf{x} \in \Omega_i$ and $M_i(\phi(\mathbf{x})) = 0$ for $\mathbf{x} \notin \Omega_i$, $i = 1,2,3$. This new function can be further expressed as follows:

$$\begin{cases} M_1(\phi(\mathbf{x})) = 1 - H(\phi(\mathbf{x})) & ,\mathbf{x} \in \Omega_1 \\ M_2(\phi(\mathbf{x})) = H(\phi(\mathbf{x})) - H(\phi(\mathbf{x}) - k) & ,\mathbf{x} \in \Omega_2 \\ M_3(\phi(\mathbf{x})) = H(\phi(\mathbf{x}) - k) & ,\mathbf{x} \in \Omega_3 \end{cases} \tag{3.1}$$

where $M_1(\phi(\mathbf{x})) = 1$ in subdomain $\Omega_1$, and $M_1(\phi(\mathbf{x})) = 0$ in subdomains $\Omega_2$ and $\Omega_3$. $M_2(\phi(\mathbf{x})) = 1$ in subdomain $\Omega_2$, and $M_2(\phi(\mathbf{x})) = 0$ in subdomains $\Omega_1$ and $\Omega_3$. $M_3(\phi(\mathbf{x})) =$

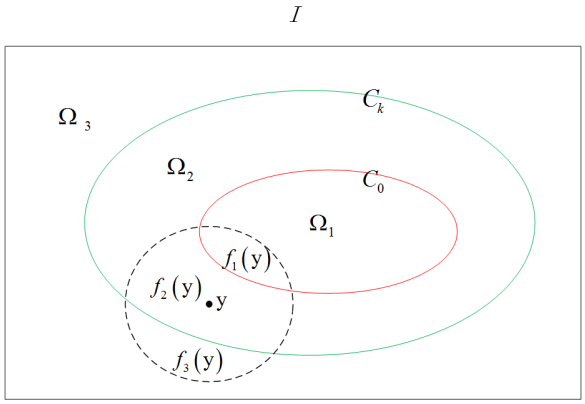


Figure 3.2: Schematic map of Level sets

1 in subdomain $\Omega_3$, and $M_3(\phi(\mathbf{x})) = 0$ in subdomains $\Omega_1$ and $\Omega_2$. This 'new-heaviside' function promises computation independence of image information from each subdomain during curve evolution process.

## 3.3. ENERGY FORMULATION

In our method, the energy functional is defined as:

$$\varepsilon(\phi) = D(\phi) + L(\phi) + R(\phi) \tag{3.2}$$

where $D(\phi)$ is data fitting term, $L(\phi)$ is contour length regularization term, and $R(\phi)$ is distance constraint and regularization term.

### 3.3.1. DATA FITTING TERM

For expressing data fitting term, region-scalable fitting (RSF) model is imposed [2]. This is a region-based level set model, and it processes the data information in a scalable region. As shown in Fig. 3.2, region inside the dashed line is the scalable area centered at $\mathbf{y}$, and $f_1(\mathbf{y})$, $f_2(\mathbf{y})$, $f_3(\mathbf{y})$ are constants that are estimated average image intensities in their local area. Therefore, there is energy functional:

$$D(\phi(\mathbf{x})) = \sum_{i=1}^{3} \lambda_i \int \left( \int K(\mathbf{x}-\mathbf{y}) \left| I(\mathbf{x}) - f_i(\mathbf{y}) \right|^2 M_i(\phi(\mathbf{x})) \, d\mathbf{x} \right) d\mathbf{y} \tag{3.3}$$

where $\lambda_i$ is the weighting coefficients, $K(\mathbf{x}-\mathbf{y})$ is kernel or window to define the size of scalable region, and $f_i(\mathbf{y}) = \frac{K*(M_i(\phi(\mathbf{x}))I)}{K*M_i(\phi(\mathbf{x}))}$, $i = 1,2,3$.

### 3.3.2. LENGTH TERM

Contour length term can be defined as $\upsilon|C|$, which aims to keep smoothness of two contours. It can be expressed as:

$$L(\phi(\mathbf{x})) = \upsilon_1 \int \left| \nabla H(\phi(\mathbf{x})) \right| d\mathbf{x} + \upsilon_2 \int \left| \nabla H(\phi(\mathbf{x}) - k) \right| d\mathbf{x} \tag{3.4}$$

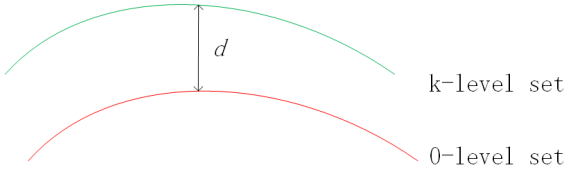


Figure 3.3: Schematic map of Level sets



where $v_1$ and $v_2$ are the weighting coefficients. $\left|\nabla H\left(\phi\left(\mathbf{x}\right)\right)\right|$ calculates the absolute gradient value of Heaviside function across 0-level set contour, which means that the sum of $\left|\nabla H\left(\phi\left(\mathbf{x}\right)\right)\right|$ along 0-level set contour is small, 0-level set contour will be smooth. Therefore, the first term is to smooth 0-level set contour, the second term is to smooth k-level set value.

### 3.3.3. DISTANCE CONSTRAINT TERM

This term is the most creative term in our method, which can not only keep curve evolution in order, but also promise distance between 0 and k level evolute smoothly. Especially, it can protect contours to converge accurately around unclear boundaries. The energy functional is expressed as:

$$R\left(\phi\left(\mathbf{x}\right)\right)=\mu\int\frac{1}{2}\left(\left|\nabla\phi\left(\mathbf{x}\right)\right|-\alpha\left(\mathbf{x}\right)\right)^2 d\mathbf{x}+\omega\int\left|\nabla\alpha\left(\mathbf{x}\right)\right|^2 d\mathbf{x}+\eta\int\left(\alpha\left(\mathbf{x}\right)-Th\right)^2 d\mathbf{x} \tag{3.5}$$

where $\mu$, $\omega$ and $\eta$ are weighting coefficients, $\alpha(\mathbf{x})$ is a distance constraint function, $Th=\frac{k}{d_c}$, and $d_c$ is a constant (in pixel) defined by physical information of LA wall thickness.

The first term in Eq.3.5 is to regularize level set function. In our method, reinitialization of level set function is not required. However, although this non-reinitialization idea originates from Li's method [3], it plays more functions in our method. In Li's method, regularization of level set function is realized by encouraging $\left|\nabla\phi\right|$ to be 1. In our method, by encouraging level set function to be $\alpha$, the level set function can also be regularized. Function $\alpha$ plays a key role in our method. Besides this regularization role, this term builds an important connection between 0-level and k-level set contours. Theory of this connection is shown in Fig.3.3. Assume that thickness between 0 and k-level set contours is $d$, so that a gradient function can be obtained as $\left|\nabla\phi\right|=(k-0)/d=k/d$. $\alpha$ is a connection between 0 and k-level set, it is also a constraint between these two contours, which can promise the distance between these two contours varies smoothly only if $\alpha$ varies smoothly.

The second term is to keep function $\alpha(\mathbf{x})$ vary smoothly and then evolution of $\phi$ can be smooth. Driven by Data fitting term, $\alpha(\mathbf{x})$ will continue evaluating, and the evolution will stop until 0 and k-level set contours lay on boundaries of objects. This can promise an accurate distance $d$ between two contours.

The third term aims to guide $\alpha$ vary in a reasonable range, which is different from DR2LS model [1]. Compared to the hard constraint of constant $\alpha$ [4], function $\alpha$ is a soft constraint to the distance between 0 and k-level contours and is more accurate and has a wide application range to objects with different thicknesses. However, in unclear

boundaries, evolution of function $\alpha$ in [1] may be easily out of control. Therefore, the parameter $Th$ is designed to hard constraint the evolution of $\alpha$, and finally only have a soft effect on distance between 0 and k level set.

## 3.4. SOLUTIONS TO ENERGY MINIMIZATION

Based on the energy functional, the curve evolution problem is transferred to convex optimization problem, which is a minimization problem. The gradient descent method can be used, where search direction and evolution step are required to be computed [5]. Besides given a starting point $\phi \in \mathbf{dom}\varepsilon(\phi)$, there are 3 steps in the gradient descent method:



Step 1: Search Direction $\triangle\phi = -\bigtriangledown\varepsilon(\phi)$

Step 2: Choose step size $\triangle t$

Step 3: Update $\phi = \phi + t \cdot \triangle\phi$

where the given starting point is initialization in our method.

### 3.4.1. EVOLUTION DIRECTION

According to gradient descent method, evolution direction to minimization of variational energy formulation are $\frac{\partial\phi}{\partial t} = -\frac{\partial\varepsilon}{\partial\phi} = -\left(\frac{\partial D}{\partial\phi} + \frac{\partial L}{\partial\phi} + \frac{\partial R}{\partial\phi}\right)$ and $\frac{\partial\alpha}{\partial t} = -\frac{\partial R}{\partial\alpha}$, so that there are:

$$\begin{aligned}\frac{\partial\phi}{\partial t} =& \lambda_1\delta(\phi)e_1 - \lambda_2\left(\delta(\phi) - \delta(\phi-k)\right)e_2 - \lambda_3\delta(\phi-k)e_3 \\ &+ \left(\upsilon_1\delta(\phi) + \upsilon_2\delta(\phi-k)\right) div\frac{\bigtriangledown\phi}{|\bigtriangledown\phi|} \\ &+ \mu\left(\bigtriangledown^2\phi - \alpha\right) div\frac{\bigtriangledown\phi}{|\bigtriangledown\phi|}\end{aligned} \tag{3.6}$$

with

$$\frac{\partial\alpha}{\partial t} = \mu\left(|\bigtriangledown\phi| - \alpha\right) + 2\omega\bigtriangledown^2\alpha - 2\eta(\alpha - Th) \tag{3.7}$$

where $\delta(\phi)$ is Dirac function which is the derivative of Heaviside function $H$. Based on the relation between integration and convolution, $e_i = (K * \mathbf{1})I^2 - 2I(K * f_i) + K * f_i^2$, $i = 1,2,3$. In each iteration, $\alpha$ and $\phi$ are alternatingly updated.

### 3.4.2. EVOLUTION STEP

As shown in section 2.2.2, the evolution step $\triangle t$ should satisfy CFL condition, where $\mu\triangle t \leq 1/4$. Since there is $\mu > 0$ in our method, $\triangle t$ can be set in a reasonable value, such as $\triangle t = 0.1$ with $\mu = 1$.

## 3.5. ANALYSIS TO KEY PARAMETERS AND COEFFICIENTS

In level set methods, parameters take a very important role, which could decide the quality of final result. Different values of parameters have different effects on the evolution,

and an excellent combination of parameters values is highly required. Based on functions of each parameter in the energy functional, the direction to obtain optimal parameters is clear.

### 3.5.1. WEIGHTING COEFFICIENTS

In our methods, there are three types of weighting coefficients. One is for usage of data, one is for curve smooth, and the last one is to regularize level set function and constraint distance between two contours.



#### DATA WEIGHTINGS

$\lambda_1$, $\lambda_2$ and $\lambda_3$ are coefficients to control weightings of three data regions $\Omega_1$, $\Omega_2$ and $\Omega_3$, which decide how many contributions data from different regions can do. As shown in Fig.1.2, SPACE-MRI has a good performance in visualization of empty LA cavity, and a poor image quality can be seen outside epicardium. Moreover, there is no clear boundary between epicardium and background. It means that data information from subdomain $\Omega_1$ can be regarded as reliable data, and information from subdomain $\Omega_3$ can not be trusted. Therefore, data from subdomain $\Omega_1$ should take domination during evolution process, which means that $\lambda_1$ should have a higher value than $\lambda_3$. In other words, reliable data in subdomain $\Omega_1$ can increase the accuracy of results, and the negative effect from non-uniform subdomain $\Omega_3$ should be decreased.

#### CURVE SMOOTH COEFFICIENTS

$v_1$ and $v_2$ can control the smoothness of 0 and k-level set curves, respectively. The difference of this two parameters should not have a key influence to the final result.

#### REGULARIZATION COEFFICIENTS

There are two functions for distance constraint term, which are regularization of level set function and distance constraints between two contours. Therefore, $\mu$ is the coefficient to regularize the level set function, $\omega$ and $\eta$ are coefficients to control weightings of distance constraints. Moreover, $\omega$ decides how important $\alpha$ should vary smoothly, and hard or soft constraint to $\alpha$ from $Th$ highly depends on value of $\eta$. There are no clear relations between values of $\mu$ and $\omega$. But the value of $\eta$ should smaller than $\omega$, otherwise, this distance constraint term will be a hard constraint like the situation when $\alpha$ is a constant.

### 3.5.2. OTHER PARAMETERS

Apart from weighting coefficients, other parameters also plays an important role in our method.

#### PREDEFINED PARAMETERS

Parameters $k$ and $Th$ should be defined before curve evolution. $k$ is a parameter that is expressed in level set function. Values of $k$ have a negligible effect on the final result, which has been proved in several papers [1, 4, 6] and also verified in our method. However, value of $k$ should be decided based on global initialization of level set function.

The size of kernel $K$ plays an important role in our method. A big size can increase the robustness for initialization, but the robustness for inhomogeneity will be decreased.

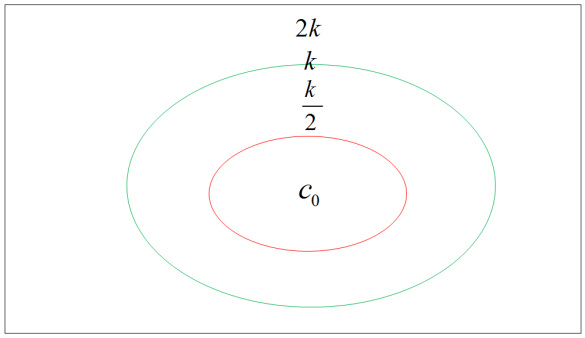


Figure 3.4: Schematic initialization of Level set function

Moreover, a big size of $K$ will heavily increase the complexity when computing convolution. Although the inhomogeneity in our datasets are not severe, a big size of $K$ is not desirable in our method.

$Th$ is a key factor in our method. Because of $Th$'s constraint to $\alpha$, distance constraints to thickness between 0 and k contours become more flexible and suitable to our problem. Based on the physical information of thickness of LA wall [7] and resolution of our image data, value of $Th$ can be set in a range from 5 to 10. And the result is not sensitive to the $Th$ value in this range.

### PARAMETERS FOR INITIALIZATION

In level set method, initialization is a vital beginning. In most level set methods, because 0 level set gradually expands or shrinks during evolution process, what objects can be detected is sensitive to the location of initial 0 level set. Therefore, the location of initial 0 level set directly decides the accuracy of final results.

The theory described above in this thesis is based on an assumption, which is that the value of level set function inside 0 level set is negative value. In our two layers level set method, since $k$ is positive value, the initial values of level set function divergent outwardly, as shown in Fig.3.4. $c_0 < 0$ is initial value of level set function $\phi$ in subdomain $\Omega_1$, $k/2$ is is initial value of $\phi$ in subdomain $\Omega_2$, and $2k$ is initial value of $\phi$ in subdomain $\Omega_3$. Although our method is not sensitive to the value of $k$, it is necessary to set a relatively big value. Because in our method, absolute value of gradient of level set function $|\nabla\phi|$ is encouraged to be corresponding value in function $\alpha$, a reasonable value of $k$ can make a clear difference among values of level set function in different subdomains. Therefore, an ordered evolution process is promised and there will be no undesirable new contours emerged.

The value of $c_0$ is also very important. Especially, if big evolution iteration times are required, it is necessary to let $c_0$ have a big absolute value. Otherwise, level set function in subdomain $\Omega_1$ may easily over-evolve and emerge new 0 level set contours.

## 3.6. COMPARISON TO FORMER WORKS

Since Vese proposed multiphase level set method in 2002 [8], several algorithms are developed to embed various prior information. However, most of them are very complicated and difficult to implement. In [1, 4], two-layer level set methods with distance regularization have been proposed, which are excellent inspirations for two-layer segmentation problems. One is a region-based level set method based on a simple function $\alpha$, the other one is a edge-based level set method based on a constant $\alpha$. These two methods are both developed to deal with left ventricle wall segmentation problems.



### CONSTANT $\alpha$

In this method, $|\nabla\phi|$ is encouraged to be a constant $\alpha$, which is a hard distance condition. Distance between 0 and k level set contours will be encouraged to be close to $k/|\nabla\phi|$. Since $k/|\nabla\phi|$ is about equal to $k/\alpha$, the distance will be fixed to a value around $k/\alpha$.

In application of two layer level set methods, the main goal is to detect the thickness between two contours. Based on anatomical information, the thickness of LA wall is not strictly a constant. Once the thickness is fixed, it is no significance to do this automatic detection. In other words, if the thickness is not equal to or around $k/\alpha$, the result will be not accurate, unless the boundary is clear enough and the data fitting term takes an absolute domination. This hard constraint constant $\alpha$ could be used in the edge-based method [4], where objects have obvious edges. But it is not easy to meet situations when there are very clear boundaries. Therefore, although this method can get a result on objects with a regular shape and clear boundaries, it heavily limits the data driven evolution process.

### FUNCTION $\alpha(\mathbf{x})$

Compared to constant $\alpha$, function $\alpha$ is required to update during each evolution iteration time. In the initialization step, function $\alpha$ is also initialized. To keep the distance between two contours evolve in order, the distance between two contours should vary smoothly. The evolution should stop when contours arrive at desirable boundaries. Moreover, the distance constraint is introduced by function $\alpha$. Therefore, function $\alpha$ should vary smoothly.

The evolution speed of level set function will slow down when 0 and k level contours are close to the actual boundaries, only if there exit clear boundaries. However, it works not well when boundaries are not clear and the levels are easily over-evolved, so that the result will be not accurate.

### NEW FOR OUR METHOD

Aiming to obtain an accurate result in all boundaries, including unclear and clear boundaries, a constraint to function $\alpha$ is proposed in our method. It can control the evolution speed when the detected distance is close to real distance, it is helpful to detect the actual boundaries.

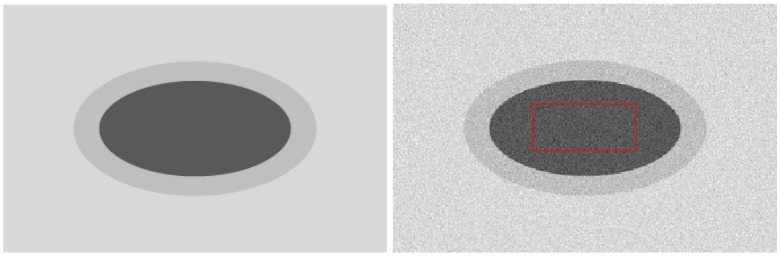

(a) Original synthetic image (b) Initialization of 0-level set contour

Figure 3.5: 0-level set initialization of synthetic image

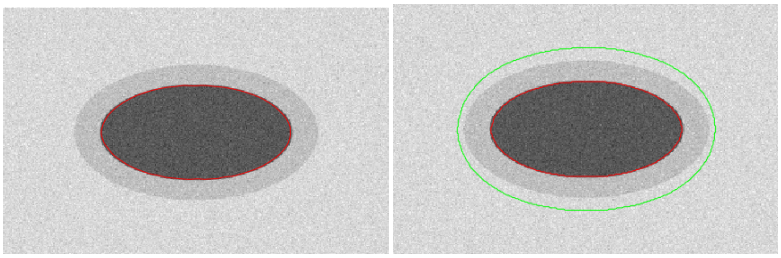

(a) The result of 0-level set contour evolution (b) Initialization of 0 and k level set contour based on the result of 0-level set contour

Figure 3.6: Initialization of two-layer level set function

## 3.7. VALIDATION TEST ON SYNTHETIC IMAGES

In this section, performance of former works and our method are tested on the synthetic image. The original image and initialization is shown in Fig.3.5. The result from one-layer level set function is applied to realize the initialization of two-layer level set function, as shown in Fig.3.6. The final results of these three methods are compared in Fig.3.7.

Noise is added to the synthetic image. The results of 3 methods are almost the same and all of them can be considered to be accurate. The reason for the same results is the clear boundaries, where the data fitting term takes the absolute domination during the evolution process and the hard constraint of constant $\alpha$ is not such hard any more.

In this synthetic image validation test, our method is verified to have a good performance, which at least has as the good performance as former works. Therefore, our method has potential to be further applied on experiment images.

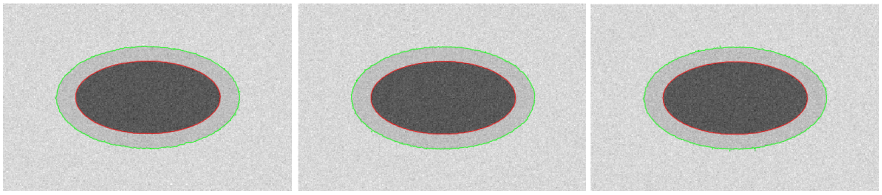

(a) The result of 'Constant $\alpha$' method (b) The result of 'Function $\alpha$' method (c) The result of our method



Figure 3.7: Comparison of 3 methods

## REFERENCES


[1] C. Feng, S. Zhang, D. Zhao, and C. Li, *Simultaneous extraction of endocardial and epicardial contours of the left ventricle by distance regularized level sets,* Medical physics **43**, 2741 (2016).

[2] C. Li, C.-Y. Kao, J. C. Gore, and Z. Ding, *Minimization of region-scalable fitting energy for image segmentation,* IEEE transactions on image processing **17**, 1940 (2008).

[3] C. Li, C. Xu, C. Gui, and M. D. Fox, *Level set evolution without re-initialization: a new variational formulation,* in *Computer Vision and Pattern Recognition, 2005. CVPR 2005. IEEE Computer Society Conference on*, Vol. 1 (IEEE, 2005) pp. 430–436.

[4] Y. Liu, G. Captur, J. C. Moon, S. Guo, X. Yang, S. Zhang, and C. Li, *Distance regularized two level sets for segmentation of left and right ventricles from cine-mri,* Magnetic resonance imaging **34**, 699 (2016).

[5] S. Boyd and L. Vandenberghe, *Convex optimization* (Cambridge university press, 2004).

[6] C. Yang, W. Wu, Y. Su, and S. Zhang, *Left ventricle segmentation via two-layer level sets with circular shape constraint,* Magnetic resonance imaging **38**, 202 (2017).

[7] R. Beinart, S. Abbara, A. Blum, M. Ferencik, K. Heist, J. Ruskin, and M. Mansour, *Left atrial wall thickness variability measured by ct scans in patients undergoing pulmonary vein isolation,* Journal of cardiovascular electrophysiology **22**, 1232 (2011).

[8] L. A. Vese and T. F. Chan, *A multiphase level set framework for image segmentation using the mumford and shah model,* International journal of computer vision **50**, 271 (2002).

# 4

# Implementation and Evaluation

## 4.1. Implementation Steps

Initialization of level set function is a very important factor in most level set methods. To obtain the best performance of our method, there are two steps in implementation of our method.

In the first step, a preliminary segmentation of endocardial contour is implemented. Because of the good quality of LA cavity, an Edge-based level set method called DRLSE is applied here [1]. In this step, a rough contour can be obtained, as shown in Fig.4.1(a).

In the second step, two-layer level set function is initialized based on the result from step 1. The location of endocardial contour from the first step is used to represent the location of 0-level set in two-layer level set function. And based on this initialization of 0-level set, the initialized location of k-level set can be defined by erosion. Since initialized locations of 0 and k level set contour are defined, initialization of our two layer level set function can be set, as shown in Fig.4.1(b).

## 4.2. Evaluation Criteria

Evaluation methods are applied to judge the performance of one method. Differences between detected results and ground-truth should be quantitative. An accurate and practical evaluation criteria is highly required. To promise the objective of evaluation results, only one evaluation is not enough. Therefore, in our method, two reliable and popular evaluation criterias are applied, which are widely used in MICCAI challenge and segmentation problems.

### 4.2.1. Dice Similarity coefficients

Dice Similarity coefficients (DSC) method is also called 'overlap' method generally. It is a method to quantify percentage of the overlapping area between detected results and ground-truth. Assume that $A$ is the detected region obtained from our method, and

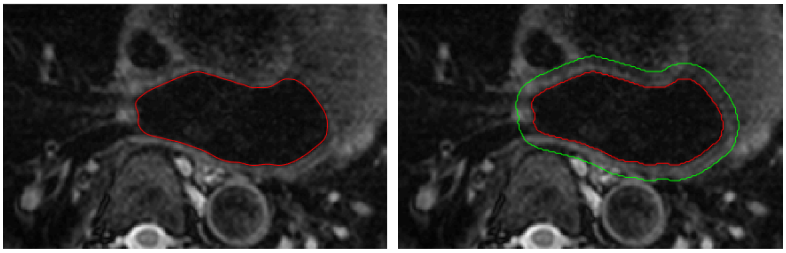

(a) The result in First step

(b) Initialization of two-layer level set function in Second step

Figure 4.1: Initialization of two-layer level set function



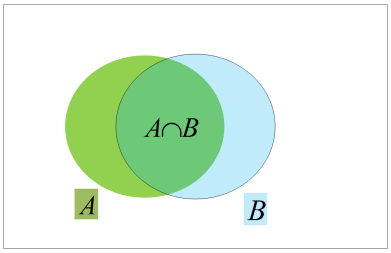


Figure 4.2: Sketch map of DSC

region $B$ is the reference in ground-truth, as shown in Fig.4.2. Therefore, the Dice Similarity coefficient can be represented as:

$$DSC = \frac{2 \times |A \cap B|}{|A| + |B|} \tag{4.1}$$

where $|A \cap B|$ is the overlapping area between region $A$ and reference B, $|A|$ is the area of region $A$ and $|B|$ is the area of reference region B.

The value of DSC is between 0 and 1. A high value of DSC means a high correlation between region $A$ and reference $B$, which represents a high accuracy of the compared method.

In our method, DSC is calculated regarding to endocardium and epicardium, respectively. These two DSCs indicate the performance on segmenting endocardium and epicardium in our method.

### 4.2.2. AVERAGE PERPENDICULAR DISTANCE

Average perpendicular distance (APD) is a parameter to quantify differences between detected contours in our method and reference contours in ground-truth. APD measures the average distance from our detected contour to the corresponding reference contour, where all contour points should be taken into account. The sckech map is shown in Fig.4.3.

The APD must be a positive value. Especially, a smaller value of APD implies a better

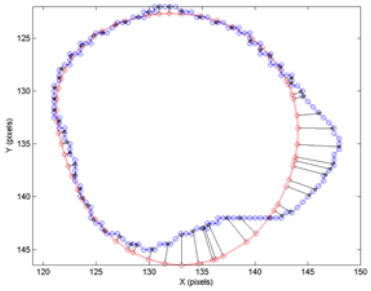


Figure 4.3: Sketch map of APD [2]



match between the detected contour and the reference contour. In other words, if the APD is smaller, the accuracy of our method is better.

In our method, APD will be computed regarding to endocardium and epicardium, respectively. The performance on segmenting endocardium and epicardium of our method will be quantified by these two APDs.

## 4.3. DATASETS

As described in section 1.1.2, the datasets we use are from SPACE-MRI. These datasets are collected by The Johns Hopkins Hospital. The machine is 1.5T Siemens Aera. Images in 2D are isotropic with 1.5mm slice thickness in 3D, the resolution is $0.625 \times 0.625 \times 1.5$ mm. Each individual slice was manually annotated by experienced clinical observers, on both endocardial and epicardial borders.

As an advanced technique, there are 10 sets of SPACE-MR LA data available. Each set of data includes 30 to 40 slices. Apart from 2 sets of data with heavy artifacts, 8 sets of data could be used. 2 sets of data ($N = 75$) are applied for training, and the rest ($N = 189$) are for testing. LA01 and LA05 are training data, LA03, LA07, LA09, LA10, LA06, LA08 are datasets for validation.

## 4.4. PARAMETERS

In section 3.5, functions and significance of parameters have been analyzed and described.

We erod the rough segmentation form first step of the endocardial region by 10 pixels as the input of our proposed two-layer level set method.

In our method, $c_0$ is -20, $k$ is set to be 20. In data fitting term, $\lambda_1 = 0.1$, $\lambda_2 = 0.001$, $\lambda_3 = 0.002$. In length term, $\nu_1 = 0.005 \times 255 \times 255$, $\nu_2 = 0.001 \times 255 \times 255$. In distance constraint term, $\mu = 1$, $\omega = 0.25$, $\eta = 0.1$, $Th = 5$ with $d_c = 4$. Given the wall thickness range of LA (1-3mm), we use $d_c = 4$ for the LA.

The evolution step $\triangle t$ is defined to be 0.1, which satisfies the CFL condition when $\mu = 1$ as described in section 3.4.2.

The kernel $K$ is a Gaussian kernel with standard deviation $\sigma = 3$, and the size of $K$ is set to be 13.

The Heaviside function is estimated as $H(\phi) = \frac{1}{2}\left[1 + \frac{2}{\pi} arctan\left(\frac{\phi}{\epsilon}\right)\right]$ with $\epsilon = 1.5$. The Dirac function $\delta(\phi)$ can be estimated as $\delta(\phi) = \frac{1}{\pi}\frac{\epsilon}{\epsilon^2+\phi^2}$, which is also the derivative of $H(\phi)$ [3]. Although the estimated Dirac function has already approximated to be an ideal Dirac function, there are still some small side lobes, which may cause that regions far away from 0 and k level sets may emerge new contours during level set function evolution process. However, because of the distance constraint term and small $\epsilon$, this interference can be almost eliminated.

The function $f_i$, $e_i$ with $i = 1,2,3$ and $\alpha$ are updated at each iteration time before updating level set function $\phi$, the formulations can be seen in section 3.3.1 and 3.4.1.

## 4.5. EFFECT OF DISTANCE CONSTRAINT



In this section, the advantage and reliability of distance constraint in our method are presented and analyzed. Compared to distance constraint in 'Constant $\alpha$' method, our constraint is proved to be more flexible and robust in more application situations.

### 4.5.1. DISTANCE CONSTRAINT IN OUR METHOD

In this section, the sensitivity of our method to value $d_c$ is examined and discussed. A weak sensitivity to the value $d_c$ will prove that the parameter $d_c$ in our method is efficient and reliable. Based on the physical information of LA wall, our method with 6 different $d_c$ values from 4 to 9 is implemented. APD and DSC of endocardium and epicardium to the ground-truth are used to evaluate accuracy of the results.

The sensitivity to values of $d_c$ of our method is indicated in Fig.4.4, which is expressed by APD and DSC. As shown in Fig.4.4(a), for 6 different integers of $d_c$, the APDs in terms of endocardium vary in a extremely small range from 0.385 to 0.408 mm, which can be considered as that different $d_c$ values have no effect on the accuracy of the detected endocardial contours. Compared to endocardial contour, the APDs in terms of epicardium shows a little bigger fluctuation from 0.583 to 0.738 mm. However, this fluctuation is very slight and smooth, which means that accuracy of detected epicardial contours is not sensitive to the value of $d_c$.

The DSCs of detected contours to the ground-truth are shown in Fig.4.4(b). DSCs in terms of endocardium are between 0.973 and 0.978, and the DSCs in terms of epicardium vary from 0.965 to 0.971. These variations caused by values of $d_c$ is really small enough and can be negligible.

Therefore, the accuracy of detected contours doesn't rely on values of $d_c$, which means that a reasonable value of $d_c$ takes a weak domination during evolution process. According to the physical information, thickness of LA wall is approximately within a range. In our implementation, it is reasonable that $d_c$ can be set as an average value of LA thickness.

### 4.5.2. DISTANCE CONSTRAINT IN 'CONSTANT $\alpha$' METHOD

In this section, 'Constant $\alpha$' method with different values of $\alpha$ is implemented. And the effect of different constants $\alpha$ is discussed.

Different from APD in other sections, the definition of APD in this section is average perpendicular distance between 0 and k level sets contours. Therefore, the relation

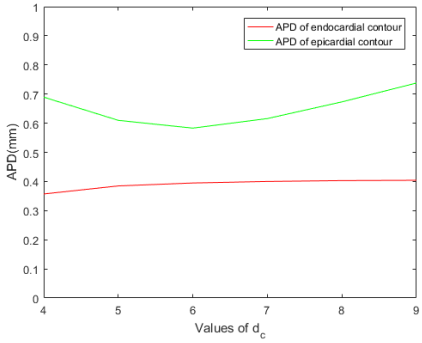


(a) Accuracy of our method in terms of APD with different $d_c$

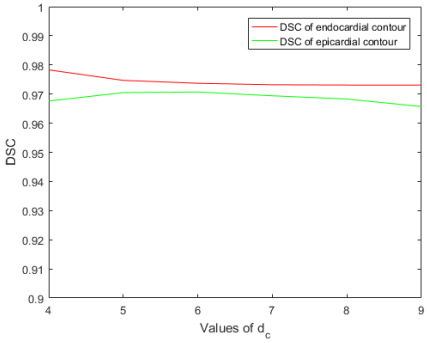


(b) Accuracy of our method in terms of DSC with different $d_c$

Figure 4.4: Results of our method with different $d_c$

between values of $\alpha$ and detected thickness can be represented. However, instead of defining values of $\alpha$, values of distance $d$ are defined here, where $\alpha$ can be calculated by $\alpha = k/d$.

The 26th slice of LA05 dataset is used as an example. The average manual (groundtruth) thickness of LA wall is 2.567 mm (4.1 in pixel), which is the basis for next comparison. Set $d$ (in pixel) to be integer from 4 to 9, the results are shown in Fig.4.6(a).

From Fig.4.5(c) to Fig.4.5(e), the epicardial contours are gradually expanding. Expanding of detected epicardial contours highly depends on the value of $d$, where a big value of $d$ will cause a big expanding of epicardial contour.

For quantitative evaluation, in 'Constant $\alpha$' method, the detected thickness of LA wall can be shown in Fig.4.6(a). The distance between detected contours increases gradually with increased $d$ values, which means that the detected thickness of LA walls highly relies on the predefined value $d$. It can be concluded that the constant $\alpha$ shows a negative effect on detecting accurate boundaries. Since thickness of LA wall can not be a fixed

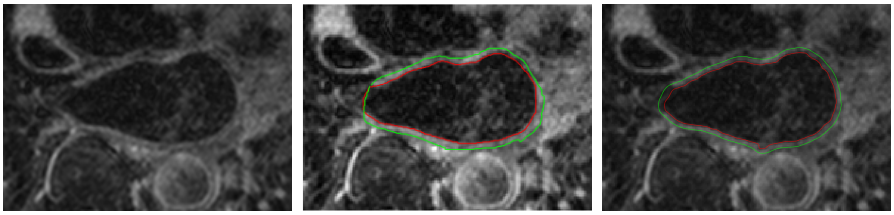

(a) Original image (b) Ground-truth (c) Result with $d = 3$

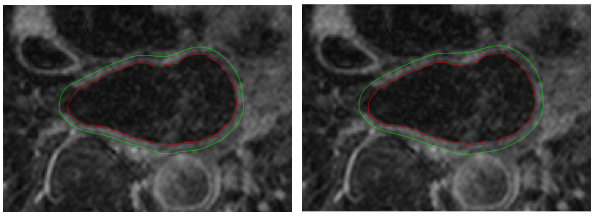

(d) Result with $d = 7$ (e) Result with $d = 10$

Figure 4.5: Results with different $d$ in 'Constant $\alpha$' method

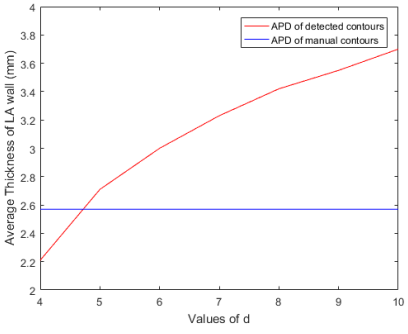


(a) Detected thickness with different $d$ values compared to groundtruth thickness in 'Constant $\alpha$' method

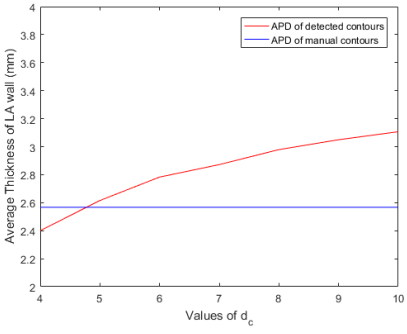


(b) Detected thickness with different $d_c$ values compared to groundtruth thickness in our method

Figure 4.6: Effects of different $d$ or $d_c$ values on detected thickness of LA wall compared between 'Constant $\alpha$' method and our method

value and has a little wider range, 'Constant $\alpha$' method can not be applied to solve our LA wall segmentation problem. Therefore, in next sections, only 'Function $\alpha$' method will be discussed.

Furthermore, results of our method with different $d_c$ values are reported in Fig.4.6(b). When $d_c$ changes from 4 to 10, detected thickness of LA wall varies slightly between 2.4 and 3.1 mm. Compared to results in Fig.4.6(a), values of $d_c$ show a much slighter and smoother effect on final results in our method. This comparison implies the outstanding advantage of our method, which is that our distance constraint is much less sensitive to values of $d_c$ than the hard constraint in 'Constant $\alpha$' method. In other words, the segmentation results in our method do not highly rely on the values of $d_c$, which is really important in detecting the real boundaries. Therefore, the feasibility and reliability of the distance constraint in our method are again proved.



## 4.6. EXPERIMENT AND COMPARISON

In this section, our training datasets are tested, and results of our method are evaluated and analyzed. Moreover, since in section 4.5.2, 'Constant $\alpha$' method has been proved to be meaningless in terms of our situation, only 'Function $\alpha$' method is taken into account in this section. Results of 'Function $\alpha$' method are compared with results in our methods.

### 4.6.1. LA01 DATASET

#### OVERVIEW

The parameters for implementation are defined in section 4.4. Our method is implemented in terms of all slices in LA01 dataset, and an example of the segmentation result from one slice is shown in Fig.4.7.

As we can see in Fig.4.7(a), although the LA cavity has a good visualization quality, the epicardium is blurry and almost mixes with boundary in some regions. Compared to groundtruth in Fig.4.7(b), the result of our method in Fig.4.7(d) shows a high agreement with groundtruth. And the evolution in regions with unclear boundaries is efficiently controlled in our method. However, the result shown in Fig.4.7(c) from 'Function $\alpha$' method has a bad performance in these regions with unclear boundaries, which can be regarded as an over-evolved process.

This comparison proves that our method has a much better performance than 'Function $\alpha$' method in regions with unclear boundaries.

One important thing should be noticed here. Because of the image quality or the special shape of LA, some parts of LA wall can not be recognized even by experienced experts. It is not possible to delineated all the contours accurately. Therefore, in regions without visualized endocardium or epicardium, experienced experts will use a straight line to represent which regions are not visualized and can not be considered in the final result, as shown in Fig.4.7(b). However, this judgment is indeed subjective and varies with different experts, and computers don't have the ability to recognize this situation. Therefore, contours which are represented by straight lines should be not taken into account in our evaluation.

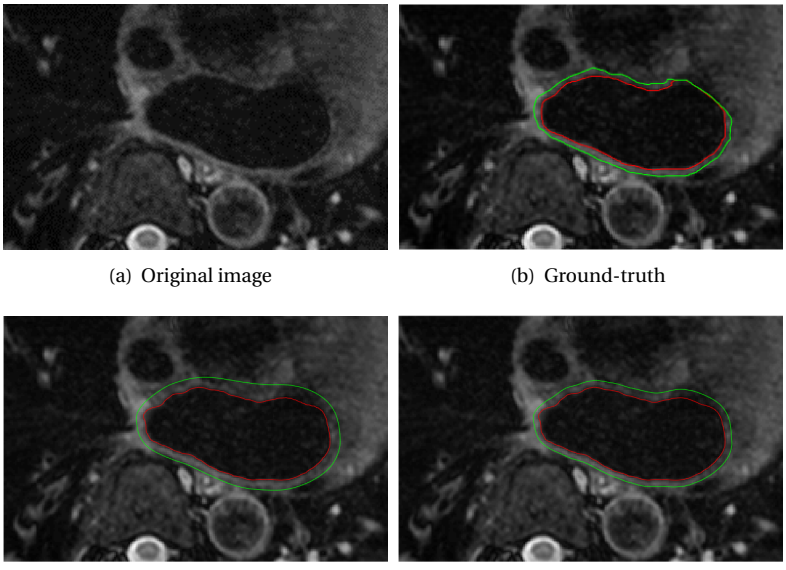

(a) Original image (b) Ground-truth

(c) Result of 'Function $\alpha$ method' (d) Result of our method

Figure 4.7: Example of segmentation result from training dataset LA01 (23rd slice)

#### QUANTITATIVE EVALUATION

In last section, a preparatory comparison is judged. In this section, quantitative evaluation and comparison are expressed, which is more reliable and intuitive. The accuracy of detected endocardial and epicardial contours is showed and discussed separately.

Evaluation results with comparison are shown in Fig.4.8. As we can see, the difference of APDs and DSCs in terms of endocardial contour is not much. Because endocardial contours are relatively clear and easy to be detected, two methods both have a good performance on detecting endocardial contours. However, compared to 'Function $\alpha$' method, our method still shows a better convergence and a higher accuracy for both APDs and DSCs in terms of endocardium.

The comparison of APDs and DSCs in terms of epicardium is shown in Fig.4.8(b) and 4.8(d). Besides a better convergence, our method performs much better than 'Function $\alpha$' method in terms of both APDs and DSCs. Because epicardial contours don't have clear boundaries with background, it is easy for 'Function $\alpha$' method to jump over unclear boundaries without constraints in our method. This result fulfills our analysis and expectation.

### 4.6.2. LA05 DATASET

Similar to training dataset LA01, results from LA05 is shown in this section.

An example of segmentation results from dataset LA05 is shown in Fig.4.9. From the anatomical image in Fig.4.9(a), more than half part of the epicardial contour is heavily blurry. It extremely increases difficulty of the segmentation problem. If evolution speed

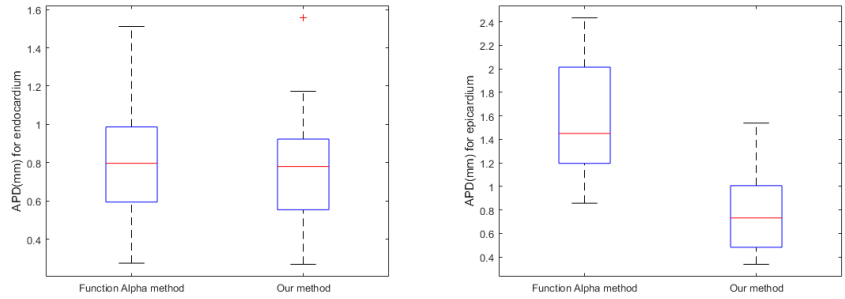


(a) APD for endocardial contour




(b) APD for epicardial contour

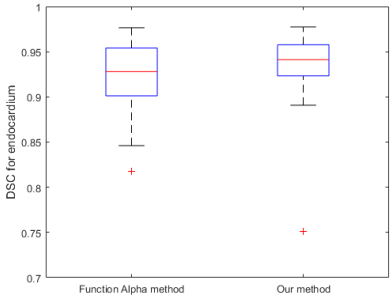


(c) DSC for endocardial contour

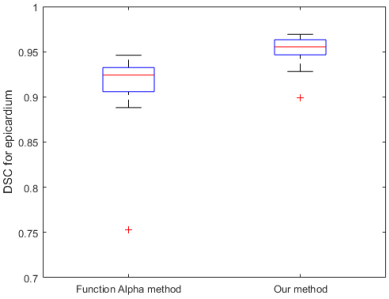


(d) DSC for epicardial contour

Figure 4.8: The accuracy of our method with comparison to 'Function $\alpha$' method on dataset LA01

can not limited when k-level sets are close to these boundaries, the over-evolution will happen with high possibility. This limitation is included in our method, but not included in 'Function $\alpha$' method. Therefore, based on observation, Fig.4.9(d) has obvious more accuracy than Fig.4.9(c).

For more intuitive statistics, boxplots in terms of APDs and DSCs are presented in Fig.4.10. APDs for endocardial contour by our method shows a little more accuracy than 'Function $\alpha$' method, which agrees with results in dataset LA01. The reason is also that endocardium is clear enough to be detected. Compared to LA01, epicardial boundaries is much weaker in dataset LA05. Therefore, the difference in terms of results for epicardium should be obvious between two methods. As shown in Fig.4.10(b) and 4.10(d), results from our method is more accurate, where APDs have smaller values and DSCs have bigger values.

### 4.6.3. OVERVIEW TO TRAINING DATASETS

In this section, results from training datasets LA01 and LA05 are quantified to values, which can be read in Table.4.1 and 4.2. The tables summarize concrete values of APDs and DSCs in terms of endocardial and epicardial contours, with mean values and stan-

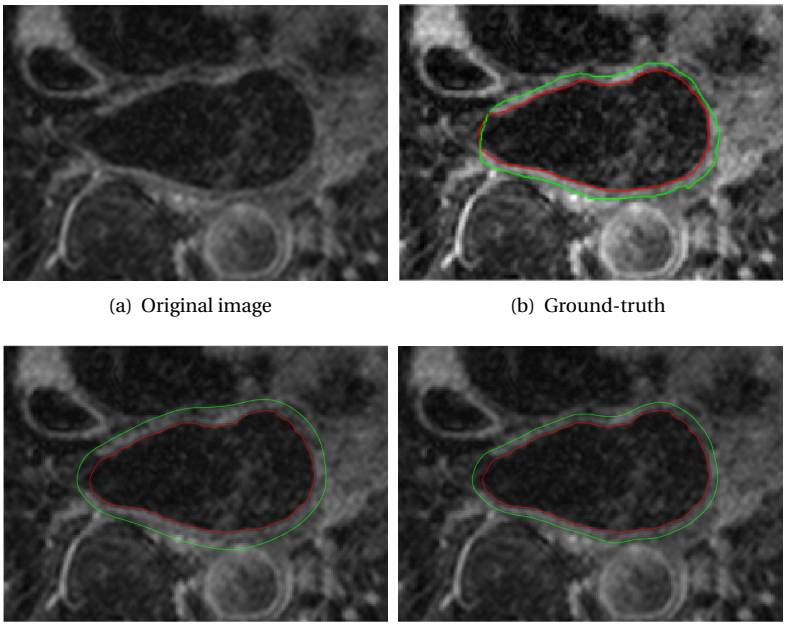

(a) Original image (b) Ground-truth

(c) Result of 'Function $\alpha$ method' (d) Result of our method

Figure 4.9: Example of segmentation result from training dataset LA05 (26th slice)

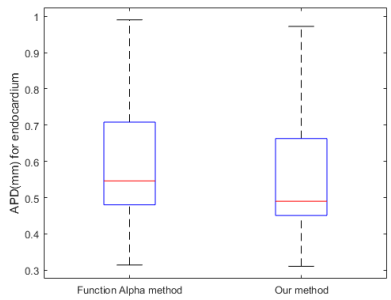


(a) APD for endocardial contour

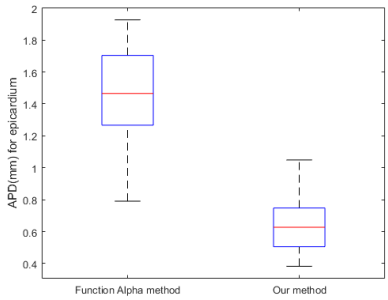


(b) APD for epicardial contour

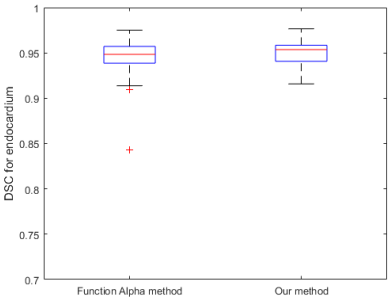


(c) DSC for endocardial contour

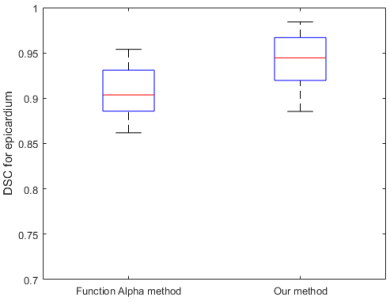


(d) DSC for epicardial contour

Figure 4.10: The accuracy of our method with comparison to 'Function $\alpha$' method on dataset LA05

Table 4.1: APDs of training datasets in terms of different methods

| Dataset | APD | | | |
|---|---|---|---|---|
| | Function $\alpha$ method | | Our method | |
| | endo | epi | endo | epi |
| LA01 | 0.828±0.437 | 1.586±0.483 | 0.764±0.266 | 0.768±0.308 |
| LA05 | 0.601±0.191 | 1.424±0.325 | 0.557±0.180 | 0.648±0.183 |

Table 4.2: DSCs of training datasets in terms of different methods

| Dataset | DSC | | | |
|---|---|---|---|---|
| | Function $\alpha$ method | | Our method | |
| | endo | epi | endo | epi |
| LA01 | 0.882±0.167 | 0.915±0.031 | 0.937±0.037 | 0.953±0.014 |
| LA05 | 0.944±0.024 | 0.908±0.325 | 0.951±0.014 | 0.943±0.027 |



dard deviation. The formula in the tables is expressed as 'mean ± standard deviation'. The 'endo' in the tables means endocardial contours, and 'epi' represents epicardial contours.

As shown in tables, the results of our method have a much better accuracy than the results of 'Function $\alpha$' method in terms of both APDs and DSCs, especially for the epicardial contours. Therefore, our methods are proved to be useful and efficient to detect both endocardial and epicardial contours. It is potential to be applied in all datasets, which is also called validation checking.

## 4.7. VALIDATION FOR ALL DATASETS

In this section, the validation of our method to all datasets is implemented and analyzed.

### 4.7.1. STATISTICAL OVERVIEW

In last section, performance of our method on training datasets has demonstrated to be excellent. However, if one method could be considered as a feasible and robust method, it is essential to test the validation on different datasets of that method. Therefore, our method is implemented on all the rest datasets, including LA03, LA04, LA06, LA07, LA09 and LA10.

For intuitive observation, APDs of endocardial contours and epicardial contours in terms of all the validation datasets are presented in Fig.4.11.

The values of APDs in terms of endocardial contours concentrate below 1 mm, which is a little smaller than APDs in terms of epicardial contours. The reason can be explained as endocardial contours in SPACE-MR LA images have a better visualization than epicardial contours. The accuracy of both detected endocardial contours and epicardial contours are good and desirable.

Values of DSCs are demonstrated in Fig.4.12. The distribution of DSCs values is smooth, and most of the values are located around 0.95. Same to the reason for smaller APDs values in terms of endocardial contours, values of DSCs in terms of endocardial

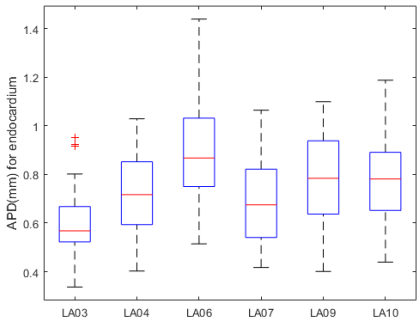


(a) APDs of our method in terms of endocardium on different datasets

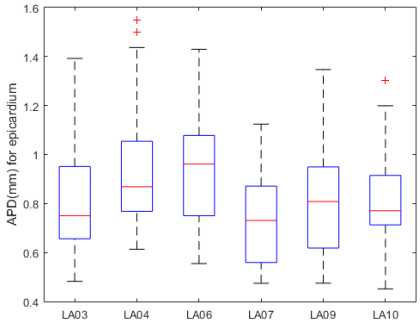


(b) APDs of our method in terms of epicardium on different datasets

Figure 4.11: APD values of our method on validation datasets

contours have a better convergence than epicardial contours.

More quantitative results are shown in Table.4.3 and 4.4, including the results of training datasets and validation datasets. Therefore, based on APDs and DSCs, our method has an excellent performance on validation data.

Furthermore, summarized statistical accuracy of results is demonstrated in Fig.4.13. This statistic implies the whole performance of our method on all datasets, and the statistical distribution fulfills our expectation.

Accuracy of results on validation datasets have an excellent agreement with training datasets, which means that our method is effective and validated. Therefore, our method has an excellent performance in detecting endocardial contours and epicardial contours in SPACE-MR LA images.Therefore, based on APDs and DSCs, our method has an excellent performance on validation data.

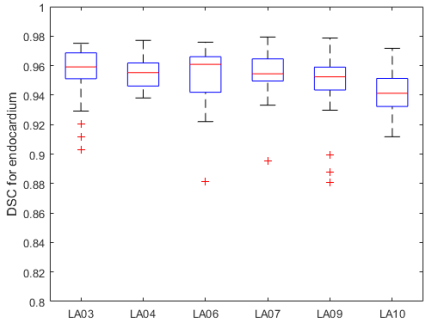


(a) DSCs of our method in terms of endocardium on different datasets

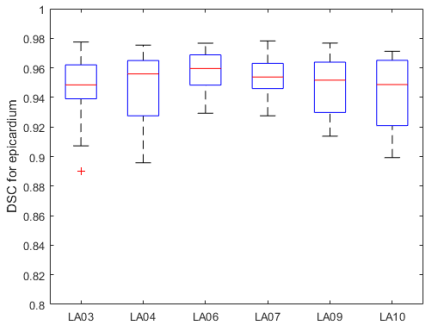


(b) DSCs of our method in terms of epicardium on different datasets

Figure 4.12: DSC values of our method on validation datasets

### 4.7.2. EXAMPLE OF SEGMENTATION RESULTS

In this section, segmentation results of different datasets are shown compared with corresponding groundtruth. In each dataset, 3 slices are selected, including one of beginning slices, one of middle slices and one of ending slices.

Examples of segmentation results of LA03, LA04, LA06, LA07, LA09 and LA10 are shown in Fig.4.14, Fig.4.15, Fig.4.16, Fig.4.17, Fig.4.18, Fig.4.19, respectively.

The sample slices of different datasets have been presented. Although the detected contours have an obvious difference in regions where there are 'double straight lines' in groundtruth, it can not be considered as an error, because these are no boundaries at all in those regions, as described in section 4.6.1. As we can see, the segmentation results have a high agreement with groundtruth. Furthermore, our method works well on majority of slices, including beginning slices, middle slices and ending slices. The accuracy and robustness of our method is proved again.

Table 4.3: Accuracy of APD in terms of training data and validation set (mean ± standard deviation)

| | Endocardial APD (mm) | Epicardial APD (mm) |
|---|---|---|
| Training datasets | 0.670±0.252 | 0.714±0.264 |
| Validation datasets | 0.748±0.207 | 0.851±0.227 |

Table 4.4: Accuracy of DSC in terms of training data and validation set (mean ± standard deviation)

| | Endocardial DSC | Epicardial DSC |
|---|---|---|
| Training datasets | 0.943±0.030 | 0.949±0.021 |
| Validation datasets | 0.952±0.018 | 0.950±0.019 |



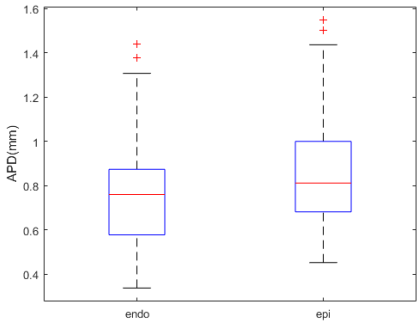


(a) The accuracy of our method for summarized datasets, with APDs evaluation

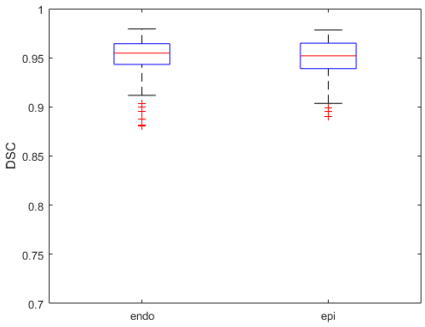


(b) The accuracy of our method for summarized datasets, with DSCs evluation

Figure 4.13: Statistical distribution of whole validation datasets

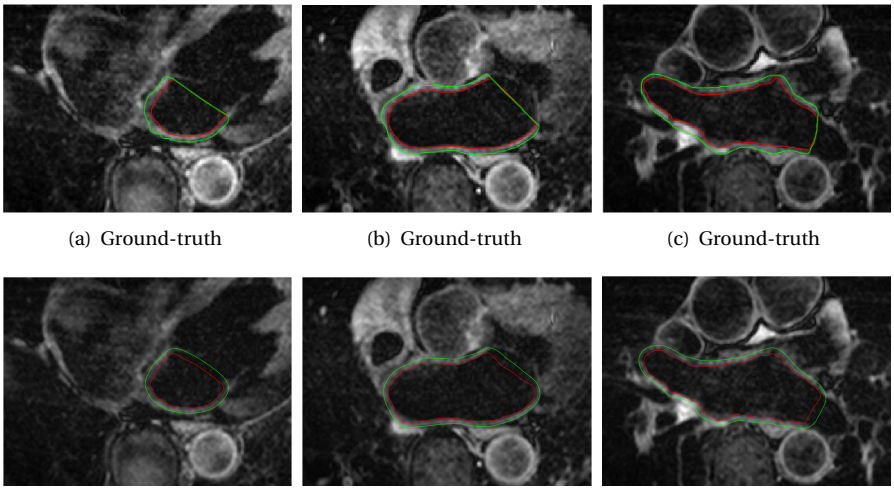

(a) Ground-truth (b) Ground-truth (c) Ground-truth

(d) Beginning slice (e) Middle slice (f) Ending slice

Figure 4.14: Examples of segmentation results of LA03 (Bottom row), with corresponding groundtruth (Top row)

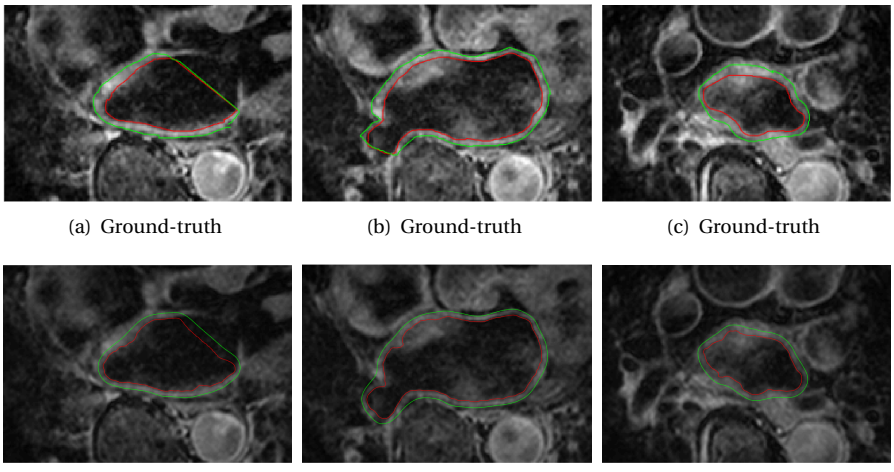

(a) Ground-truth (b) Ground-truth (c) Ground-truth

(d) Beginning slice (e) Middle slice (f) Ending slice

Figure 4.15: Examples of segmentation results of LA04 (Bottom row), with corresponding groundtruth (Top row)

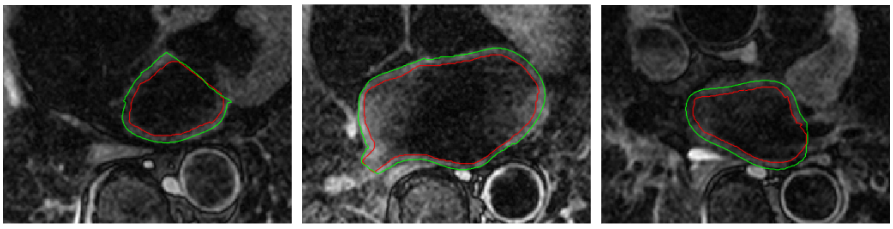

(a) Ground-truth (b) Ground-truth (c) Ground-truth

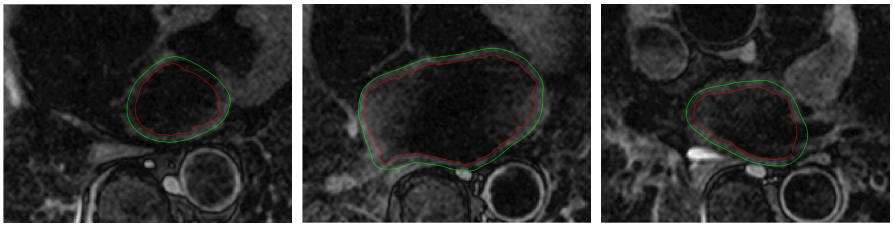

(d) Beginning slice (e) Middle slice (f) Ending slice

Figure 4.16: Examples of segmentation results of LA06 (Bottom row), with corresponding groundtruth (Top row)

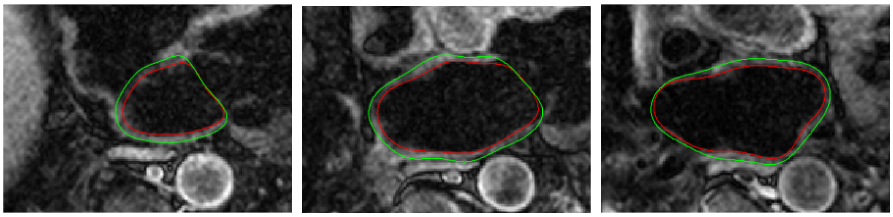

(a) Ground-truth (b) Ground-truth (c) Ground-truth

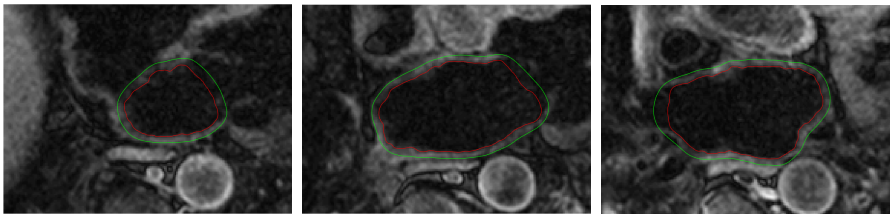

(d) Beginning slice (e) Middle slice (f) Ending slice

Figure 4.17: Examples of segmentation results of LA07 (Bottom row), with corresponding groundtruth (Top row)

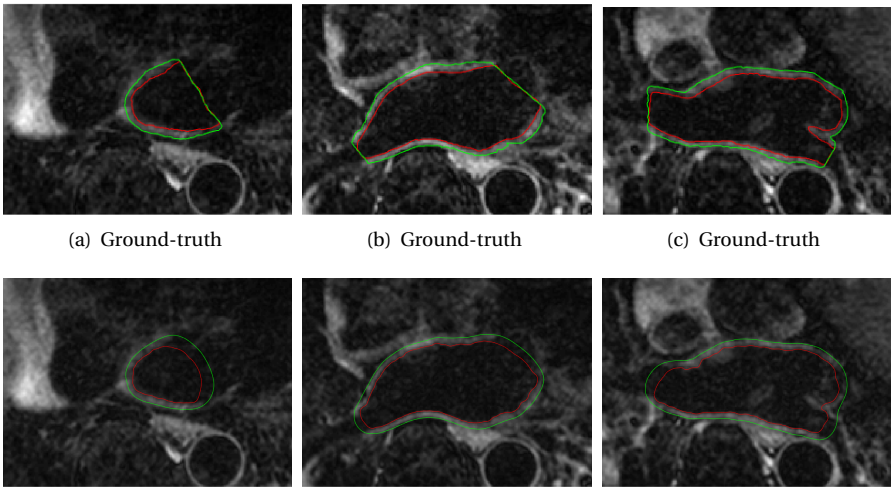

(a) Ground-truth (b) Ground-truth (c) Ground-truth

(d) Beginning slice (e) Middle slice (f) Ending slice

Figure 4.18: Examples of segmentation results of LA09 (Bottom row), with corresponding groundtruth (Top row)

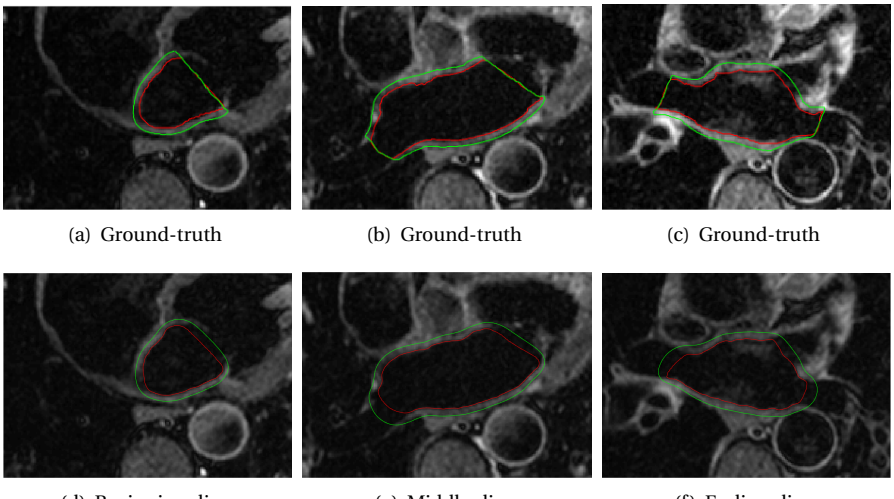

(a) Ground-truth (b) Ground-truth (c) Ground-truth

(d) Beginning slice (e) Middle slice (f) Ending slice

Figure 4.19: Examples of segmentation results of LA10 (Bottom row), with corresponding groundtruth (Top row)

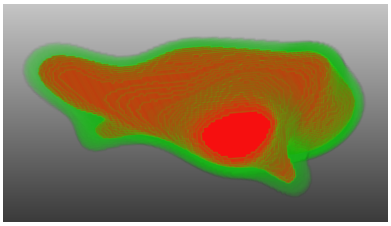

Figure 4.20: An example of segmentation results of 3D

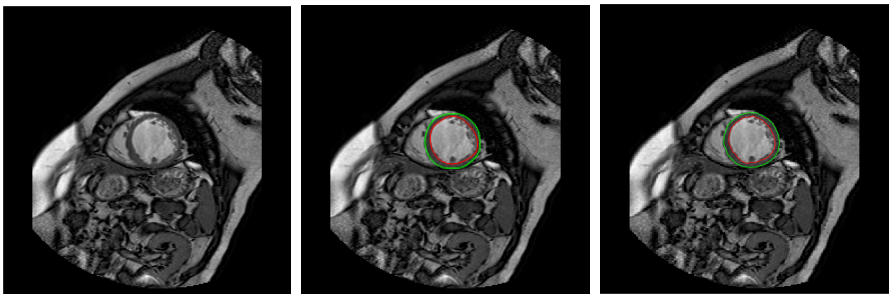

(a) Original image (b) Ground-truth (c) Result of our method

Figure 4.21: An example of segmentation results of LV data



## 4.8. EXTENSION TO 3D

Our above works solve segmentation problems based on 2D image. Normally, if we assemble segmentation results of 2D slices into 3D view, the adjacent contours may not be continuous. Therefore, in order to obtain a more continuous 3D surface contours, our method is extended to 3D problem. And dataset LA01 will be used as an example in this section. The contours in 3D are continuous and shows two smooth surfaces, as shown in Fig.4.20.

## 4.9. APPLICATION TO LEFT VENTRICLE (LV) IMAGES

In this section, our method is extended to solve LV segmentation problems. As described in section 1.3, MRI CINE LV images have a better visualization quality than LA images. However, if our method can successfully used in LV images, our method would be widely applicable. In total, 131 short-axis MRI CINE LV images at end-diastole (ED) with resolution $1.75 \times 1.75$ mm are used. Given the wall thickness range of LV (10-20 mm), we used different $d$ values with the LA, $d_c = 8$ for the LV. Moreover, besides $d_c$, only values of $\lambda_1$, $\lambda_2$ and $\lambda_3$ need to be modified when we extend our method from LA application to LV application. The example segmentation results are shown in Fig.4.21.

The segmentation results of our method show a high agreement with ground-truth. The quantitative evaluation is applied by APD and DSC methods, as presented in Fig.4.22 and Table.4.5, 4.6. The APDs in terms of endocardial contours and epicardial contours

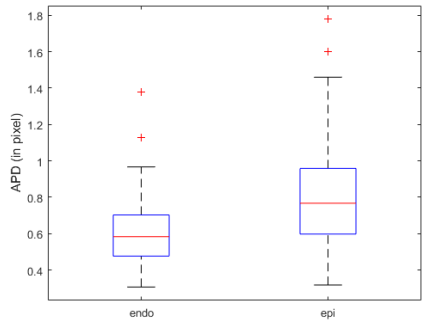


(a) Accuracy of our method in terms of APD

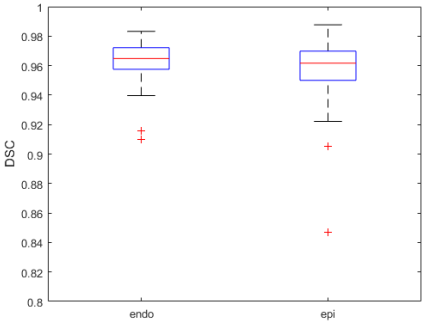


(b) Accuracy of our method in terms of DSC

Figure 4.22: Evaluation results of our method on LV data

are both around 1 pixel. The corresponding DSCs show a good performance with almost all values around 0.95.

Table 4.5: Accuracy of APD in terms of LV (mean ± standard deviation)

| | Endocardial APD (mm) | Epicardial APD (mm) |
|---|---|---|
| LV data | 1.053±0.318 | 1.391±0.426 |

Our method can be applied on LV data and has an excellent performance, which means our method can be easily extended to more kinds of data and is potential to be widely applicable.

## 4.10. DISCUSSIONS

From above sections, the breakthrough in our method compared to former methods is presented and proved to be reliable. After testing in training datasets, our method is applied to validate validation datasets. With same defined parameters to training datasets,

Table 4.6: Accuracy of DSC in terms of LV (mean ± standard deviation)

| | Endocardial DSC | Epicardial DSC |
|---|---|---|
| LV data | 0.964±0.012 | 0.962±0.020 |

our method has an excellent performance on segmenting validation datasets. For checking the applicability and robustness, our method is extended to LV data at end-diastole. The accuracy of results is within a desirable range.

## REFERENCES

[1] C. Li, C. Xu, C. Gui, and M. D. Fox, *Distance regularized level set evolution and its application to image segmentation,* IEEE transactions on image processing **19**, 3243 (2010).

[2] *Evaluation methods of lv segmentation challenge,* http://smial.sri.utoronto.ca/LV_Challenge/Evaluation.html, mICCAI CHALLENGE, 2009.

[3] T. F. Chan and L. A. Vese, *Active contours without edges,* IEEE Transactions on image processing **10**, 266 (2001).

# 5

# CONCLUSION

In this thesis, background of our LA segmentation problem is firstly analyzed. Aiming to solve the LA wall segmentation problem, a two-layer level set method is proposed to detect two contours (endocardial contour and epicardial contour) simultaneously. Especially, an efficient distance constraint is introduced, which has been proved to be feasible and reliable. With the distance constraint, the evolution speed of the level set function around boundaries is effectively limited, so that even unclear boundaries could be detected without over-evolution. Moreover, the proposed distance constraint term not only regularizes the level set evolution at two levels, but also guarantees the distance between two level sets contours varies smoothly. Compared to other state-of-art methods, the advantage and feasibility of our method are demonstrated. Experiment with quantitative and qualitative evaluations proves that our method has a good performance and robustness in segmenting LA walls. Furthermore, our method is extended to LV segmentation, and the accuracy of results is within a desirable range. In the future, our method is potential to apply in more anatomical structures segmentation problems from medical image analysis.

# ACKNOWLEDGEMENTS

This thesis thanks for patient instructions from Dr. Qian Tao, Dr.Ir. Rob J. van der Geest, Prof.dr.ir. Boudewijn P. F. Lelieveldt, and the whole members in Division of Image Processing (LKEB). Both working environment and academic instructions left me an unforgettable memory.

In TU Delft, I learned how to study for new knowledge and got solid theory background. TU Delft gives me enough freedom to study what I am interested on, and teaches me how to build a serious academic attitude. The teachers and classmates are all very nice and friendly, which organizes an excellent studying environment.

In LKEB, I learned how to apply my knowledge to solve practical problems. It affords me a great platform to touch state-of-art techniques. Besides knowledge related to my thesis, some advanced research directions like deep learning all impressed me a lot. There are so many successful researchers in LKEB. Every time when I talked with Phd candidates or researchers, I can obtain new knowledge. The experience in LKEB extremely broadens my horizons.

Sincerely, I must say thank you to my supervisors, my teachers, my friends and my family. With the help of them, I can have the opportunity to get a Msc. diploma and especially the precious experience.

*Yuanbo Ji*
*Delft, July 2017*